Heliyon

Review Article

Recent advancements in compact layer development for perovskite solar cells

Hamideh Mohammadian-Sarcheshmeh, Mohammad Mazloum-Ardakani[*]

Department of Chemistry, Faculty of Science, Yazd University, Yazd, 89195-741, Iran

[*] Corresponding author.

E-mail address: mazloum@yazd.ac.ir (M. Mazloum-Ardakani).

Abstract

Herein, we will present recent progress in the compact layer (CL) or hole blocking layer (HBL) which is known as an important layer and not as an essential layer for perovskite solar cells (PSCs). The CL involves an effective role to enhance efficiency in PSCs. Thus, any change, modification, and replacement in this layer will have a profound effect on the performance and improvement of some characteristics such as photo-stability, durability and hysteresis effect. These changes can improve the applications of PSCs in the flexible cell, industrial mass production, high-scale manufacturing. In this review, we will present recent studies on CLs.

Keyword: Energy

1. Introduction

Energy consumption is rising and energy sources, especially fossil fuels, are finishing. Therefore, the demand for renewable, accessible energies has increased significantly. After discovering the photovoltaic effect in 1839 [1], solar cells appeared and attracted a lot of attention to convert solar energy into electricity. Among the various types of solar cells, PSCs were more important and impressive because perovskite materials, used as a light absorber in PSCs, have excellent advantages

such as a great light absorbing capability, small exciton binding energy, direct band gap, and outstanding charge carrier mobility [2, 3, 4, 5]. PSCs structures include a conductive substrate such as fluorine doped tin oxide (FTO), an electron transport layer (ETL) which involves a compact layer (CL) and a mesoporous scaffold layer (for mesoporous PSCs), perovskite layer as an absorber, hole-transporting material (HTM), and a metal electrode. There are two structures for PSCs. Mesoporous PSCs (MS-PSCs) structures and planar (P-PSCs) structures. In usual MS-PSCs, mesoscopic scaffold layer formed by small size TiO_2 NPs creates a structure with little spaces which restricts perovskite grains growth inside TiO_2 scaffold and produces many voids, results to augment carrier recombination and leakage currents in PSCs. Therefore, Quasi-mesoscopic PSCs (QMPSCs) are induced as the other kind of PSCs suggesting enough big spaces to grow superb quality perovskite layer with big grain size and fewer voids [6, 7]. In P-PSCs devices, mesoporous scaffold layer is removed and ETL only includes CL. They can operate well due to the ambipolar nature of perovskite [8]. P-PSCs devices involve the simplest structure and fabrication processing due to removing high temperature sintered mesoscopic layer. Also, P-PSCs can be fabricated with a low-temperature process, which is suitable for making flexible solar cells [9, 10, 11, 12]. Many efforts have been made to improve the efficiency and stability of solar cells, which contain many studies on various layers in PSCs structures. In this review, we are focused on articles presented for CLs. The CL or HBL or ETL is a critical layer in the PSCs because it hinders the direct contact between the holes, made in perovskite layer or HTL, and FTO. Therefore, it will diminish charge recombination and augment the open-circuit voltage (V_{OC}) [13, 14, 15]. It should be pointed that charge recombination will decrease charge collection ability, the short-circuit current (J_{SC}) and the fill factor (FF) as well as V_{OC} in PSCs [16]. The CL is an electron selective layer which can collect the photo-generated electrons from the perovskite layer and transport electrons toward FTO [17, 18]. Therefore, it is essential that CLs involve compact uniform films without pinholes and cracks to obtain high efficient PSCs [19]. Furthermore, CLs with optimized thickness are very essential [20]. A thick CL will increase the distance of electrons to transport from the perovskite layer to the FTO, leads to decrease the charge transport. But a thin CL will not cover the FTO effectively. Thus the FTO layer contacts with the perovskite layer directly, leads to the charge recombination with formed holes in the perovskite layer. The optimized thickness of TiO_2 as a CL reported via traditional methods, the spin-coating method, is 50−100 nm [20]. In fact, CL thickness is related to the balance between hole blocking capability and carrier transport loss. Full coverage and adequate thickness increase hole blocking ability. Suitable film thickness decreases the carrier transport loss [21]. An appropriate CL should include some properties, such as reduced transport resistance which enhances electron extraction, good transparent in the visible light region, appropriate conduction band (CB) level which matches CL energy levels with the perovskite layer well to decrease energy loss. In addition to, superior electron

mobility, low-temperature preparation process are important [22, 23, 24]. However, in inverted PSCs which ETL placed promptly on top of the perovskite layer instead of HTL, the ETL should fully cover the perovskite layer to protect the perovskite layer from deleterious oxygen and moisture effects. Also, the used solvents in the deposition process of the ETL should be considered [25, 26, 27, 28]. The TiO_2 layer, as a famous CL, has been used from dye-sensitized solar cells (DSSCs) generation to PSCs [29, 30, 31, 32, 33, 34, 35]. The TiO_2 as an intrinsic n-type semiconductor along with a wide band gap exhibits a substantial role in augmenting electrons transportation and preventing recombination phenomenon between the FTO and HTM layer. It contains advantages such as chemical stability, inexpensive and suitable CB. But, TiO_2 has disadvantages such as low electron conductivity due to low carrier density and low electron mobility which can produce unsuitable charge transport in the perovskite [36]. Also, the photoactive nature of TiO_2 CL indicates a detrimental effect on perovskite layer stability [37]. Moreover, Snaith et al. [38, 39] showed that the charge traps and the oxygen vacancies in the TiO_2, activated by ultraviolet (UV) light, can decrease the efficiency of converting light into electricity and power conversion efficiency (PCE) in PSCs. Therefore other materials were proposed to replace TiO_2 to improve its properties. It's important to be mention that conventional methods for fabrication TiO_2 CLs such as spin-coating and spray pyrolysis need a high-temperature sintering procedure which increases the costs and stops the fabrication of flexible devices. Other methods such as atomic layer deposition (ALD) [16], electrochemical deposition [40, 41], high pressure pressing [42], and chemical bath deposition (CBD) [43] could not utilize low temperature processing. In this review, we will present PCSs with different CLs which involve various morphologies, fabrication methods and also some PCSs structures without CL. The presented articles can provide appropriate solutions to solve disadvantages and problems in the CLs.

2. Main text

2.1. Replacing of TiO_2 CL with various CLs

As previously mentioned, the TiO_2 CL indicates low electron extraction owing to its relatively poor carrier mobility. So, semiconductors with higher carrier mobility are used to replace them. Wang et al. [44] used Cadmium selenide (CdSe) nanocrystal as ETL or CL for P-PSCs due to its high electron mobility (more than TiO_2), solution-processing ability at low-temperature sintering (140 °C) and tunable band gap [45, 46, 47, 48]. An average PCE = 11.7% obtained which was higher than that of the P-PSCs devices with TiO_2 as CL (9.0%). However, both devices showed the obvious hysteresis. The existence of a hysteresis effect, lack of similarity of J-V curve which observes by changing the direction and scan rate, will reduce the accuracy of measured performance. Dong et al. [49] reported SnO_2-CL-based MS- PSCs by

the sol-gel method which showed higher J_{SC} than that of TiO_2 CL based MS- PSCs, due to higher mobility and electrical conductivity of SnO_2 than that of TiO_2. In addition, the SnO_2-CL devices indicated a faster Photoluminescence (PL) decay than that of the TiO_2-CL devices. Because SnO_2-CL has high efficient carrier extraction as a result of higher carrier mobility or lower CB level of SnO_2-CL. Nevertheless, high charge recombination in SnO_2-CL devices decrease V_{OC} and fill factor (FF) in comparison to TiO_2 devices. Dong et al. [50] employed a CL including a blended-interfacial-layer (BIL), composed of FTO, SnO_2, TiO_2, and perovskite in MS-PSCs. The FTO layer was adorned with salient spots of SnO_2 nanocrystals. FTO-SnO_2-based MS-PSCs indicated smaller series resistance (R_s) and larger shunt resistance (R_{sh}) in comparison to the FTO/TiO_2-based ones. Consequently, charge recombination decreased effectively and the dark current increased in FTO-SnO_2 compared with FTO/TiO_2-based ones. The PCE (18.16%) was higher than that of TiO_2/FTO MS-PSCs (PCE = 17.27%). Also, the hysteresis effect this device improved compared with that based on TiO_2 CL. However, the MS-PSCs (without SnO_2 CL or TiO_2 CL) indicated serious hysteresis due to the high recombination. In structures of FTO-SnO_2 and FTO-TiO_2 without mesoporous scaffold, FTO-SnO_2 based structure exhibited better durability. Because TiO_2 can excite by UV light easier than SnO_2 which causes TiO_2 operates as a photocatalyst, as a result, accelerates the decomposition of perovskite. Another kind of metal oxides is zinc oxide. The ZnO CL with low temperature solution-process has good electrical property and high charge mobility. But, ZnO CL showed poor thermal stability. Some strategies were used for the improvement of instability: using high-temperature for the exclusion of excessive OH^- groups and residual chemicals on the ZnO surface [51], aluminum doping to modify its interface property [52] and deposition of polymers between the perovskite and ZnO layers to prevent direct interaction [53]. Zhao et al. [54] utilized aluminum-doped zinc oxide (AZO) as CL which showed the PCE value of 12.6% similar to P-PSCs with TiO_2 CL but with an outstanding thermal stability. AZO devices improved stability in comparison to ZnO devices (low-temperature-processed) and ZnO nanoparticles devices (sintered ZnO nanoparticles at 400 °C). Deprotonation of the methylammonium cation by the ZnO surface produces methylamine and PbI_2. Deprotonation of the methylammonium cation (available in perovskite structure) occurs more easily at ZnO surfaces while deprotonation is difficult in AZO, owing to this fact that the acidic property of ZnO has increased by doping of aluminum. The more acidic metal oxide surfaces provide more thermal stability [51]. In fact, the enhancement of the thermal stability was related to a decrease in the Lewis acid-base reaction between perovskite and CL. The prominent conductivity and transmittance of AZO layer introduced it as a good transparent conductive electrode where was used instead of FTO and ITO in a simple cell structure: glass/AZO/perovskite/Spiro-OMeTAD/Au. In comparison with expensive ITO and FTO which is difficult to etch, AZO is low-cost and easy to etch. Also, the work function of AZO was 4.6 eV which provides a good charge transfer between

perovskite and AZO and so a great electron collection efficiency. The studies have indicated that ZnO as a CL shows some advantages, high electron-transport property, relatively wide bandgap, and electron mobility better than that of TiO_2 [21, 55, 56, 57, 58, 59, 60]. The high electronic mobility enhances the photo-generated electron transport and therefore provides the fabrication of PSCs devices without hysteresis. But, the existence of charge recombination in interfacial of the ZnO/perovskite decreases the efficiency. Furthermore, ZnO/perovskite interface shows the little chemical stability especially, at a temperature above 90 °C. Because, the methylammonium (MA^+) cations in perovskite material can be quickly deprotonated by ZnO, release methylamine and decompose the perovskite film [51]. As a result, the passivation of ZnO surface (as CL) can improve the stability and efficiency of PSCs, as well as remove the hysteresis effect. Cao et al. [61] passivated ZnO surface by a thin MgO layer and protonated ethanolamine (EA), providing a CL with a great electron transporting and results in a hysteresis-free, stable and efficient PSC (Fig. 1). High hole-blocking property of MgO would diminish the charge recombination at ZnO/perovskite interface [62, 63] and hence, promoted stability and cell performance. During EA coordination with Mg, the proton on the hydroxyl end group of EA is quickly eliminated [64]. Mg onto ZnO surface will convert the neutral chelation structure in EA into a charged monodentate structure. The charged monodentate structure provides accessible protonated amine groups for fabricating of electrostatic interaction between NH_3^+ and I^- from perovskite, elevating the great electron transport from perovskite to ZnO and providing PSCs with efficiency up to 20.05% with no hysteresis effect. Instead of conventional TiO_2 CL, a composite of ZnO/Zn_2SnO_4 was used by Li et al. [65] in PSCs through spray pyrolysis. ZnO involves an excellent electronic mobility ($205-300$ cm^2 V. s^{-1}) than that of Zn_2SnO_4 (ZSO) ($10-15$ cm^2 V. s^{-1}) [65, 66]. Also, ZSO compound is a transport-conducting oxide with high electron mobility and stability [67]. Moreover, ZnO/ZSO CL optical transmittance is better than that of TiO_2 CL. Thus the ZnO/ZSO CLs have better optical feature. In comparison to the TiO_2 CLs, the ZnO/ZSO CLs indicate higher J_S, due to the better electron collective capability and higher carrier mobility, therefore
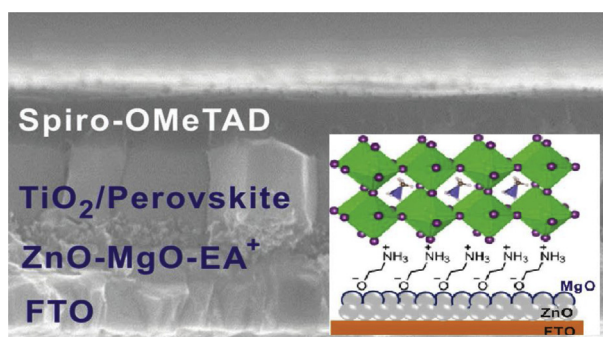

Fig. 1. Cross-sectional SEM image of a MS-PSC device with ZnO−MgO−EA$^+$ as ETL. (Reprinted with permission from Ref. [61]. Copyright 2018 John Wiley & Sons, Inc).

improve the photovoltaic performance. J_{SC} improves from 16.77 mA/Cm^2 (MS-PSC with TiO$_2$ CL) to 19.71 mA/Cm^2 (M-PSC with ZnO/ZSO CL) and PCE improves from 10.19% to 12.03%. More distinct PL quenching phenomenon happened for MAPbI$_3$/ZnO/ZSO/FTO structure which was attributed to more easily the photo-generated electrons extraction in the ZnO/ZSO CL due to the suitable energy band level. CB level of ZnO/ZSO locates in the lower level than that of TiO$_2$, thus electron injection increases from mesoporous TiO$_2$ to ZnO/ZSO CL. In spite of promising performance, V_{OC} is lower than that of TiO$_2$ CL devices. It is attributed to the recombination in ZnO/ZSO CL because of higher roughness confirmed by atomic force microscopy (AFM) results. Nevertheless, R_s for ZnO/ZSO CL cell is lower than that of TiO$_2$ CL cell, because of smaller thickness and higher carrier mobility of the ZnO/ZSO CL. One of the other materials used as CLs is Quantum dots (QD). QD such as PbS, CdSe, and CdS QDs exhibited pinhole-free and thickness-controllable CLs by using the spin-coating method [68, 69]. Also, Tu et al. [70] demonstrated a pinhole-free and ultrathin CL based on TiO$_2$ quantum dots (QDs) with high crystallization and 3.6 nm diameter. PSCs performance was examined by spin-coating three kinds of materials with a similar thickness about 50 nm: colloidal TiO$_2$ QDs (QD CL), titanium diisopropoxide bis (acetylacetanoate) precursor solution (TAA CL), and aqueous TiCl$_4$ (TiCl$_4$ CL). TiCl$_4$ CL, TAA CL and QD CL PSCs show PCE of 12.54%, 14.01% and 16.98%, respectively. The performance improvement for the TiO$_2$ QD CL PSC is attributed to an increment of FF and V_{OC}. as a result of small R_s, and large R_{sh}. Impedance spectroscopic (EIS) indicated the lowest R_s and the highest R_{sh} value for device-based QD CL. The lowest R_s is related to the lower contact and the bulk resistance in QD CL. The highest R_{sh} value shows reduction in short circuits or current leakages [71]. Lower R_s and higher R_{sh} create a higher FF and a large electron mobility [72]. QD CL PSCs exhibit large charge injection properties and small internal resistance. The reason for the various charge collection features is such defects as Ti^{3+} ions, residual chemicals, and hydroxyl groups [73]. Gao et al. [74] modified TiO$_2$ nanorod arrays (TiO$_2$-NAs) by chalcopyrite CuInS$_2$ quantum dots (CuInS$_2$ QDs) through solvothermal method. The CuInS$_2$ QDs are photovoltaic materials with suitable bandgap (1.6 eV) and high absorption coefficient (105 cm^{-1}), as well as little toxicity [75]. Because, the CL and valence band (VB) of chalcopyrite CuInS$_2$ QDs are matched appropriately with that for TiO$_2$ and perovskite, therefore, charge transfer from perovskite to the TiO$_2$ CL and light harvesting can be enhanced, which improves device performance. The rough surface of the QD-modified TiO$_2$ nanorods, in comparison to the smooth surface of the unmodified TiO$_2$ nanorods, can create a bigger surface area and superior contact with the perovskite film. Consequently, many channels will be produced by the utilization of TiO$_2$-CuInS$_2$-NAs for the charge collection and transportation. This QD-modification promotes the light absorption and improves the perovskite crystallization. The best PCE = 11.7% acquired by optimized the QD growth time (12 hours, layer thickness of 8 nm) which was higher than PCE value for a cell using

nanoarrays without QD modification (PCE = 8.9%) [76]. A solution-processed carbon quantum dot (CQDs)/TiO$_2$ composite was used by Li et al. [77] as a CL in P-PSCs. CQD is a kind of carbon nanomaterials composed of separate, quasi-spherical nanoparticles with sizes lower than 10 nm, which presents good light harvesting property and promising optical, electrical features [78]. The CQDs enhance the energy levels matching between the perovskite and TiO$_2$ CL that improves electron mobility and electron extraction between the TiO$_2$ and perovskite layers. Thus enhance J$_{SC}$ (21.36 mA. cm^{-2}). With the optimized CQDs amount (10 wt %), the average PCEs of PSCs enhanced from 12.7% to 17.5%. By using of CQDs/TiO$_2$ CL, the hysteresis effect is suppressed due to the efficient charge transport at the perovskite/TiO$_2$ interface and the decreased electron transport potential barrier between perovskite and CL interface [79]. In addition to metal oxides, fullerene, and its derivatives (C$_{60}$, PC$_{61}$BM, ICBA, and PC$_{71}$BM) are extensively utilized as electron extraction materials in the low-temperature fabrication of PSCs [80, 81, 82]. The performance of PSCs with these fullerene materials did not show large improvement, except PC$_{71}$BM. Furthermore, PC$_{61}$BM is expensive and shows variable performances due to the lack of morphological controllability under sintering conditions [83]. In comparison with PC$_{61}$BM and metal oxides, n-type organic small molecules [84] have gotten much attention as ETL, because they can be synthesized easily and modified for matching their energy levels with the perovskite energy levels. Besides, introducing sulfur species into their molecular structure is very easy, which leads to enhance the interfacial reaction between the perovskite and the ETL via S-Pb or S-I bonding [85, 86]. Wang et al. [87] utilized sulfur-containing n-type small molecule hexaazatrinaphtho[2,3-c] [1,2,5]thiadiazole (HATNT) as CL or ETL in low-temperature and solution-processed P-PSCs. Fig. 2 shows synthetic routine of HATNT. Device with HATNT indicates higher V$_{OC}$ and J$_{SC}$ in comparison to the device with PC$_{61}$BM as CL. This high V$_{OC}$ is attributed to the more perfect band
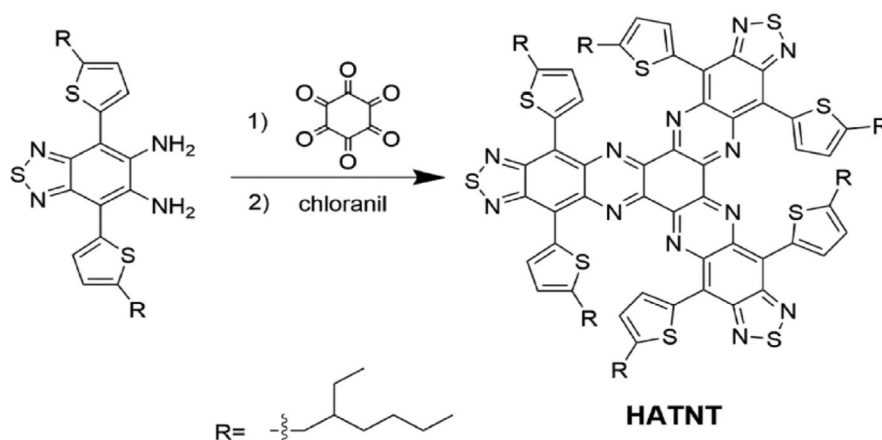

Fig. 2. Synthetic routine of HATNT. (Reprinted with permission from Ref. [87]. Copyright 2017 John Wiley & Sons, Inc).

alignment between CL and the MAPbI$_3$ film. In fact, the superficial lowest unoccupied molecular orbital (LUMO) level in the HATNT produces a superior electrically contact with the MAPbI$_3$ layer, leading to a larger potential difference between the electron and hole and transport layers (higher V$_{OC}$) [56, 88]. The electron mobility of the HATNT (1.73×10^{-2} cm^2 V^{-1} s^{-1}) is higher than that of the PC$_{61}$BM, which has an important role in increasing J$_{SC}$ in HATNT devices. Interfacial interaction between the perovskite and the HATNT via S-I or S-Pb bonding [85, 86] and effective suppression of photo-generated charge recombination at the perovskite/CL as well as high V$_{OC}$ and J$_{SC}$ are useful to improve devices performance. PCE = 16.2% for PC$_{61}$BM-based device improves to PCE = 18.1% for HATNT device. Devices with molecules PC$_{61}$BM or HATNT show slight hysteresis because the perovskite and these molecule clusters cannot quickly penetrate into each other [89], thus decrease ions motion in the perovskite and hysteresis effect. An important topic about the TiO$_2$ CL is the presence of deep trap states on its surface which creates a high leakage current and charge recombination. A predominant strategy to decrease these trap states in order to produce highly efficient PSCs is interface engineering. Shahiduzzaman et al. [90] showed interfacial engineering of TiO$_2$ CL by a thin layer (10 nm thickness) of N-phenyl[60]fulleropyrrolidine (PNP) which was an inexpensive organic material with a simple one-step solution-processing. The PNP is used as an interfacial modifier for TiO$_2$ CL instead of using expensive PCBM. Modification, improved perovskite crystallization, and enhanced charge mobility and electrical properties for TiO$_2$. Also, charge separation improved from perovskite layer to the ITO electrode, because of perfect alignment of PNP energy levels with perovskite energy levels. As a result, J$_{SC}$ with PNP became higher than that of PCBM (from 11.90 to 21.44 mA cm^{-2}). The PNP indicated larger contact angles of water droplets than PCBM, because of the hydrophobic nature of the phenyl group in PNP. Thus, moisture entrance into the perovskite layer strongly was prevented in PNP devices. In fact, the PNP interfacial layer between TiO$_2$ and perovskite layers augmented the value of photo-generated charge carrier sites and decreased the trapping of charges and accumulation at the TiO$_2$ interface. These effects enhanced photovoltaic parameters of the PNP devices compared with those of devices without PNP. J$_{SC}$ enhanced from 11.90 to 21.44 mA cm^{-2}, FF from 0.49 to 0.56 and PCE enhanced from 5.12 % to 8.38%. It is worthwhile to mention that CLs with higher CB level than FTO CB level indicate an outstanding blocking effect. Thus, charge recombination blocking effect for any passivation layer depends on CB level of utilized material. Nb$_2$O$_5$ with a more negative CB than that of TiO$_2$ is effective for blocking of recombination. The Nb$_2$O$_5$ was used as an excellent CL in MS-PSCs (Al$_2$O$_3$ as a mesoporous layer). The device with Nb$_2$O$_5$ CL presented significantly higher V$_{OC}$ (1.11 V) than that of the device with TiO$_2$ CL. This was ascribed to high recombination blocking effect by Nb$_2$O$_5$ CL, which was proven from the dark smaller current. Because, Al$_2$O$_3$ is an insulator, dark current moves by electron transport from FTO to the Spiro-OMeTAD layer or the

perovskite layer. This result proposes that Nb_2O_5 CL blocks recombination much better than TiO_2 CL. Nevertheless, J_{SC} in Nb_2O_5 CL cell was smaller than that of the TiO_2 CL cell, because the Nb_2O_5 CL slightly hinders electron transfer from perovskite to FTO. Thus, thinner and denser Nb_2O_5 CL should be used to decrease resistance and the electron injection barrier from perovskite to FTO in order to further improvement of the cell performance, J_{SC}, FF and PCE [91]. Tan et al. [92] reported a strategy for contact-passivation by chlorine-capped TiO_2 nanocrystal. Anatase TiO_2 nanocrystals (NCs) with a diameter ~ 5 nm were synthesized via a nonhydrolytic method and then Cl-capped TiO_2 NCs (TiO_2-Cl) with 12 % of Cl respect to Ti atoms were produced through the reaction of benzyl alcohol with $TiCl_4$ at 85 °C [93, 94]. The perovskite films quality and charge transfer on both CLs (TiO_2-Cl, TiO_2 without passivation) were the same. This suggests that quality and interfacial charge transfer are not the major reasons for improving performance by TiO_2-Cl. The charge recombination lifetime (t_r) in a TiO_2-Cl device was predominantly higher than that of the TiO_2 device. It means slower charge recombination at the TiO_2-Cl/perovskite interface. Density functional theory (DFT) results proved that interfacial Cl atoms decrease deep trap states formation on the perovskite surface, as a result, enhance surface passivation and decrease recombination at the TiO_2/perovskite contact. Also, The Cl atoms produce powerful electronic coupling and chemical binding at the TiO_2/perovskite P-PSCs [95]. Consequently, hysteresis-free P-PSCs with PCEs of 20.1% for small-area devices (0.049 cm^2) and 19.5% for large-area devices (1.1 cm^2) were obtained. The developing of low-cost, easy and low-temperature processes for fabrication of TiO_2 CLs with high electron extraction ability to create PSCs with high PCE and without hysteresis effect, have been attracted much attention. Byranvand et al. [96] reported TiO_2 CL modified with p-type ionic salt CuI by a simple one-step spin-coating process (CuI@TiO_2). CuI is an inexpensive and stable hole conductor [97]. Electrons cannot be extracted via the CuI islands because the CB energy of CuI (-2.2 eV) is higher than that of perovskite (-3.93 eV). However, they can be predominantly extracted to the TiO_2 layer at interface formed between perovskite and TiO_2 layer. The p-type nature of CuI, containing small Cu$^+$ and large I$^-$ ions at the interface between perovskite and TiO_2 CL, hinders the back-recombination and enhances electron extraction. In addition, the higher conduction and valence band energy levels of CuI in comparison with those of TiO_2 can induce a shift of TiO_2 band edge and decrease trap states density. Thus, increase the V_{OC} and FF values in devices. Since the recombination rate (hundreds nanosecond scale) is much slower than the extraction rate (tenths nanosecond scale) [98] even if a part of the generated holes moves to CuI, positive CuI can pull the electron to the interface between TiO_2 and perovskite layer which enhances electron extraction and decreases nonradiative recombination (Fig. 3). The optimized device indicates negligible hysteresis, which is attributed to removing trap sites and high electron extraction by CuI@TiO_2 as a CL. In fact, the improvement in the PCE (PCE = 13.5% for unmodified CL to PCE = 19% for modified CL) was related to

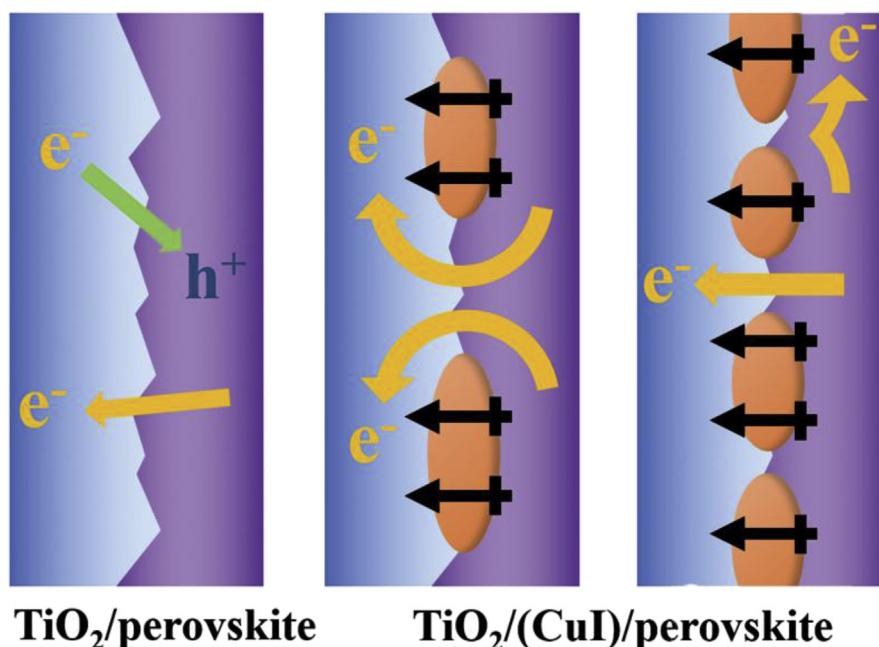TiO₂/perovskite   TiO₂/(CuI)/perovskite

Fig. 3. The figure of interface with various amount of CuI islands. Without CuI, electron−hole recombination occurs easily, and with CuI, electrons are pulled to the interface between the perovskite and TiO$_2$ and are extracted owing to the formed dipole moment. However, too many CuI islands on TiO$_2$ block the electrons passway. (Reprinted with permission from Ref. [96]. Copyright 2017 John Wiley & Sons, Inc).

the p-type nature of CuI, which can pull electrons in the direction of the perovskite/ TiO$_2$ interface, leading to a shift of the energy levels and prominent electron extraction with a low trap density.

It should be mentioned that the decomposition and deterioration of the perovskites via moisture can be affected by CL. Li et al. [99] utilized a composite of large π-conjugated graphdiyne (GD) into cross-linkable fullerene [6,6]-phenyl-C61-butyric styryl dendron ester (C-PCBSD) as a CL. Graphdiyne (GD), as a large π-conjugated carbon material involves a natural band gap and stiff 2D network. Also, (C-PCBSD) material has been employed in polymer solar cells and PSCs accompanied by high long-term stabilities [100, 101, 102]. The strong π−π interaction between the two highly π-conjugated GD and C-PCBSD in the CPCBSD: GD composite produced the C-PCBSD molecules to have an ordered stacking with a face-on direction (Fig. 4), which is beneficial for electron transfer and perovskite growth with a higher crystalline and multiple ordered crystal direction parallel to the C-PCBSD: GD substrate. This improves perovskite crystallization, leading to efficient charge transport and high J$_{SC}$ (23.30 mA/cm^2). The C-PCBSD: GD film involved superb electron mobility (over 6 times improvement in the electron mobility for C-PCBSD), suitable energy-level and efficient charge extraction. The increment of V$_{OC}$ (from 1.06 V to 1.11 V) is attributed to the alignment effect of C-PCBSD in tailoring the energy
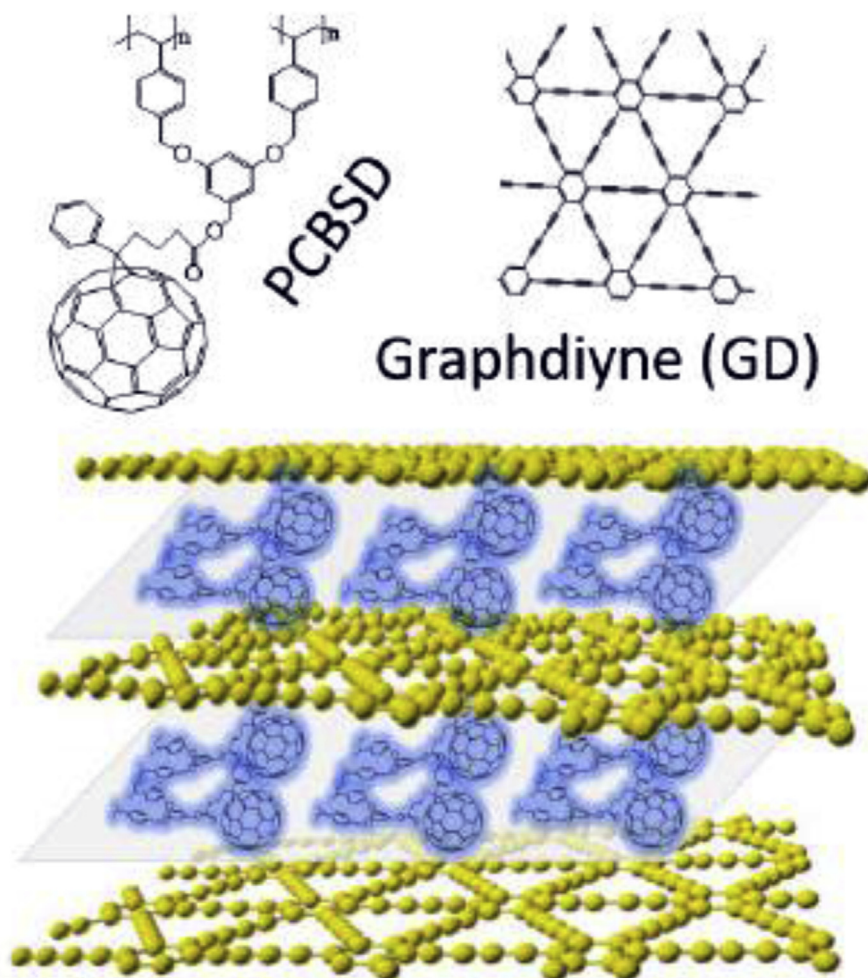
Fig. 4. Molecule structures of PCBSD and Graphdiyne and schematic illustration for the face-on stacked C-PCBSD film owing to the π-π stacking interaction between. (Adapted from Ref. [99] with permission of Elsevier).

levels between the TiO_2 and perovskite layers. It should be noted that cell stability extremely depends on the surface wetting features. The contacting angles of water on TiO_2/C-PCBSD: GD and TiO_2 were 97.2° and 8.9°, respectively. This shows that C-PCBSD: GD films have a poor wettability. As a result, the C-PCBSD film can form an adhesive film with suitable moisture resistance, which can prevent the decomposition of the perovskites by moisture. Thus, C-PCBSD: GD film provides more stability. In addition to moisture stability, UV stability is also important. Superior UV stability is very significant when devices involve outdoor applications, extremely in places with higher altitudes than ground level and space regions. Where UV light is usually intensive [103]. The low stability of TiO_2-based PSCs under UV irradiation can be ascribed to the light-provided desorption of absorbed oxygen in TiO_2 surface [104] and also, the large photocatalytic activity of TiO_2 [37]. In fact, TiO_2-based PSCs indicate an intrinsic instability against UV irradiation, where

oxygen adsorbed at surface oxygen vacancies reacts with photo-generated holes in TiO_2, producing deep traps. These oxygen vacancies at TiO_2 surface (either rutile or anatase phases) operate as deep traps for charge recombination under UV irradiation [8]. In addition, UV-induced degradation of the perovskite film at the TiO_2/perovskite interface happens due to a high photocatalytic reaction on the defective sites of oxygen vacancies upon band gap excitation of TiO_2, resulting in the decomposition of the perovskite thin film. Some methods have been suggested to increment of the UV light stability such as, the using of UV inactive inorganic materials instead of TiO_2 such as Al_2O_3 [104], utilization of down-shifting materials on TiO_2 [105], using mesoporous SnO_2 as CL [106], utilization of a buffer layer as a modifier between TiO_2 and perovskite layer such as CsBr [37, 107], and using alternative BL such as La-doped $BaSnO_3$ to increase PSCs photo-stability [108]. It is mentioned that PSCs with TiO_2 as CL decrease the UV light stability. However, the using of iron (III) oxide as CL shows a significant improvement in photo-stability because of the low photocatalytic activity of iron (III) oxide. Luo et al. [109] used iron(III) oxide as ETL. Cell structure involved in situ grown α-Fe_2O_3 nanoislands on the compact α-Fe_2O_3 which deposited on FTO layer by a one-step deposition method. Iron(III) oxide (α-Fe_2O_3) is one of the most thermodynamically stable iron oxides with n-type semiconducting features [110]. Because of its much lower CB level energy($\approx 0.3\,eV$) in comparison to TiO_2 [111], it is a good electron extraction material. Also, high charge recombination rate and low diffusion lengths of the hole [112] are useful to decrease the photocatalytic activity of α-Fe_2O_3 and enhance the UV stability. The geometry of α-Fe_2O_3 nanoislands film leads to excellent light transmittance, because the gaps between nanoislands enhance enough light transmittance and nanoislands size and increase the light scattering phenomenon. Also, α-Fe_2O_3 nanoislands film leads to large surface area contact to perovskite, and thus sufficient electron extraction. The high electron transport from the perovskite to the nanoisland-based film prevents negative ionic carrier accumulation at the perovskite/α-Fe_2O_3 interface, which leads to a negligible hysteresis [113, 114, 115]. A promising PCE (18.2%) obtains which is larger than that of the PSCs with these CLs, Zn_2SnO_4 [116], WO_x [117], ZnO [21], SnO_2 [36,72], and CdS [118], as well as organic phenyl-C_{61}-butyric acid methyl ester (PCBM) [119]. Chen et al. [120] also, utilized an atomic stacking transporting layer (ASTL) based on 2D atomic sheets of titania ($Ti_{1-\delta}O_2$) as a CL. 2D atomic sheets of titania ($Ti_{1-\delta}O_2$) operate as a superior high-κ dielectric material with $\varepsilon_r > 100$ even at thicknesses with a few nanometers [121]. They are fabricated by the exfoliation of an original layered $K_{0.8}Ti_{1.73}Li_{0.27}O_4$ crystal via a mild chemical process [121, 122]. The atomic sheets of 2D titania, indicate the negligible density of oxygen vacancies with a larger band gap and expanded UV transparency, thus show much better UV stability compare to traditional TiO_2 CLs. They are useful for fabrication of flexible PSCs due to no high-temperature sintering process. Liu et al. [123] presented stacking n-type materials, TiO_2 and SnO_2 as CL in P-PSCs. The Stacking of TiO_2 (deposited by spray

pyrolytic) and SnO_2 (deposited by spin coating aqueous colloidal) together can provide higher performance than that of bilayer devices [124, 125] and popular CLs (TiO_2 or SnO_2). It indicates a PCE = 18.03% without hysteresis effect and a long-term stability ($\sim$91% efficiency >90 days at 30% relative humidity without encapsulation). In addition to stability under a harsh condition with intense UV illumination, at 60 °C, 60% humidity is better than that of single TiO_2 and SnO_2 CLs. There are many oxygen vacancies or Ti^{3+} sites at TiO_2 surface. Long time UV irradiation can react with oxygen in the air and induce an unstable charge transfer complex [126]. The hole in the VB, on bandgap extraction of TiO_2, can be recombined with the electron at the oxygen site and leads to desorbing the oxygen [104]. This creates a free electron in the CB and a positively charged oxygen vacancy site at the TiO_2 surface, then the free electron can be recombined with the excess holes rapidly. However, the suitable alignment between the highest occupied molecular orbital (HOMO) of HTL and the stacked n-layer CB can result in excellent electrons extraction (Fig. 5). Therefore, the defects generated at TiO_2/perovskite interfacial will be passivated and the hole transfer to TiO_2 is completely prevented by SnO_2, which decreases recombination. Consequently, the stability and the performance improve by passivating of the defective interface. In TiO_2 CLs with lower charge mobility and shallower CB level, happen more electron accumulation at the interface of TiO_2/perovskite, thus show a severe hysteresis with inferior efficient. By inserting a layer of SnO_2 between the layer of TiO_2 and perovskite, SnO_2 can be fully used to gather and transfer charge. Stacked n-layer shows negligible hysteresis in comparison to that of a pure TiO_2 sample. One type of PSCs is the flexible cell. The plastic substrates were used in flexible PSCs instead of glass substrates. However, the poor thermal stability of plastic substrates leads to challenges for flexible PSCs. As a result, fabrication of ETLs or CLs with a room temperature processing is critical.
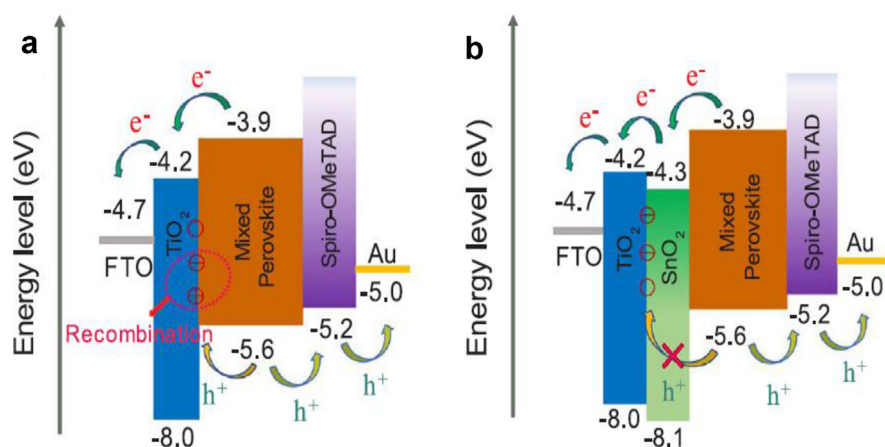

Fig. 5. (a) Diagram of energy levels of TiO_2 with other functional layer in the device according to their energy band. (b) Diagram of energy levels of stacked n-layer with other functional layer in the device according to their energy band. (Adapted from Ref. [123] with permission of Elsevier).

Chu et al. [127] demonstrated utilization of modified ZnO CL with a [BMIM]BF$_4$ ionic liquid (IL-BF$_4$) on a cheap substrate (PET/ITO) by a room temperature solution method. [BMIM]BF$_4$ ionic liquid modification extremely decreases the contact barrier between ZnO and perovskite and increases the carrier mobility (three times). Therefore enhances the charge extraction and significantly lowers the photoelectron loss. In addition to, it creates perovskite film with larger and more homogeneous grains and great crystallinity owing to the smoother interface with high wettability (high hydrophilic IL-BF$_4$). Furthermore, modification of ZnO CL by 0.05% IL-BF$_4$ produces dipolar polarization layer between the ZnO CL and perovskite, leads to energy level tailoring and the charge extraction enhancing. Thus, flexible PSC indicates a maximum J$_{SC}$, V$_{OC}$, FF as well as a maximum PCE of 12.1% (1.4 times of the non-modified one). Mahmud et al. [128] demonstrated highly stable, low-temperature sol-gel processed ZnO CL modified with 2% cesium compounds such as CA (cesium acetate) and CC (cesium carbonate). Modification with CA (Zn-CA CL) produces perovskite with large grain due to the pinhole-free, compact and smooth surface of the underlying CA. But, Modification with CC (Zn-CC CL) produces perovskite with smaller grain because of the dendritic grain morphology of the underlying CC. Photovoltaic parameters for Zn-CA CL devices are superior to those of Zn-CC CL. The high V$_{OC}$ in Zn-CA CL devices is related to higher grain size perovskite film on top of CA film which decreases recombination. However, lower V$_{OC}$ in Zn-CC CL devices is related to rough perovskite surface topography (10.50% higher than perovskite at CA) which creates a shunting path in Zn-CC CL [129]. The high J$_{SC}$ in Zn-CA CL devices is related to the high n-type conductivity of CA and low electron injection barrier for the photo-generated electrons from perovskite layer to Zn-CA CL which provides more efficient electron extraction capability [130]. Electrode polarization phenomena are suppressed in larger grain sized perovskite in Zn-CA CL devices, thus, these devices show reduced photo-current hysteresis effect. Besides, the stability of Zn-CA CL device is 400% higher than that of Zn-CC CL. Hu et al. [131] used a low temperature ($\sim 100\ °C$) solution process for fabrication of cerium oxide (CeO$_x$) as an ETL instead of PCBM in inverted PSCs. CeO$_x$ is an inexpensive n-type semiconductor with a wide bandgap, good transparency, and high-temperature stability. Comparing to PCBM, CeO$_x$ enhanced the carrier extraction by a better energy level adjustment with the perovskite. Also, CeO$_x$ indicated a supreme hole blocking ability due to its lower HOMO level energy. Compared to PCBM ETL, a dense CeO$_x$ can perform as a diffusion barrier for protecting perovskite against moisture and metal electrode against corrosion. Thus, CeO$_x$, devices are further stable than PCBM devices. Kim et al. [132] developed a naphthalene diimide (NDI)-based polymer with strong electron withdrawing dicyanothiophene (P(NDI2DT-TTCN)) as ETL (Fig. 6) in inverted PSCs instead of the PCBM ETL. NDI has the highest electron-withdrawing backbones and strong electron transport features. In addition, the dicyanothiophene is a strong electron accepting unit, because of the introduction of the strongly
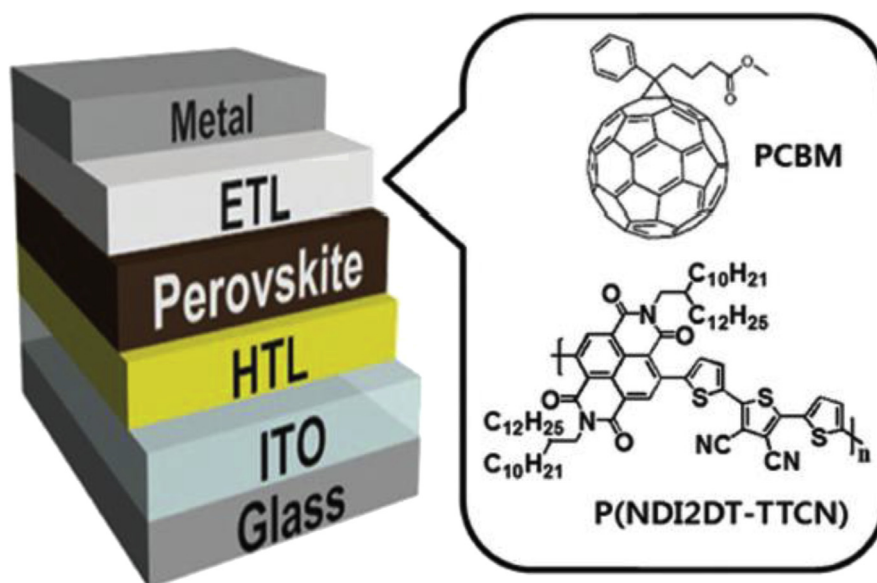
Fig. 6. Schematic illustration of the device architecture based PCBM and P (NDI2DT-TTCN), respectively. (Reprinted with permission from Ref. [132]. Copyright 2018 John Wiley & Sons, Inc).

electron-withdrawing dicyano group. Comparing to PCBM film, P(NDI2DT-TTCN) film can form an ordered $\pi-\pi$ stacking with face-on orientation among the polymer chains more effectively. As a result, it will increase better vertical charge transport than the PCBM film and indicate good electron transport. The performance of P(NDI2DT-TTCN) device (PCE = 17.0%) is higher than that of PCBM device (PCE = 14.3%), which is the highest photovoltaic performance with negligible hysteresis in polymeric ETLs. Choi et al. [133] introduced a thin film of heteropolytungstate, lithium silicotungstate ($Li_4SiW_{12}O_{40}$), produced by a low temperature (150 °C) solution process as CL in P-PSCs. Heteropolytungstates are a polyanionic nanocluster with a cage-like framework structure combined with tungsten oxide octahedral and a hetero-metal ion placed at the center of the framework. Among different heteropolytungstates, silicotungstate ($SiW_{12}O_{40}^{4-}$) involves high electron mobility. Also, $SiW_{12}O_{40}^{4-}$ can be prepared simply by a solution process at low temperatures. The crystallographic structure of $SiW_{12}O_{40}^{4-}$ (Fig. 7a) includes four $W_3O_{10}^{2-}$ clusters and one Si^{4+} ion located at the center of the framework. The FTO substrate should be modified to deposition of $Li_4SiW_{12}O_{40}$ (Li-ST) on FTO. At first, positive charges were created on the FTO layer by using hydrochloric acid, then, the substrate was inserted into an L-lysine aqueous solution. In this step, the L-lysine carboxyl group (a short-chain amino acid) is joined to the FTO substrate, while the positive amine group is standing upward from the FTO. Therefore, the hydrophobic surface of the FTO changes to a highly hydrophilic surface. In fact, the wettability of FTO glass improves. Finally, $SiW_{12}O_{40}^{4-}$ polyanion of Li-ST can be connected to the NH_3^+ terminal group of L-lysine by electrostatic attraction (Fig. 7b). As a result, a thin Li-ST buffer layer can fully cover the surface of the FTO
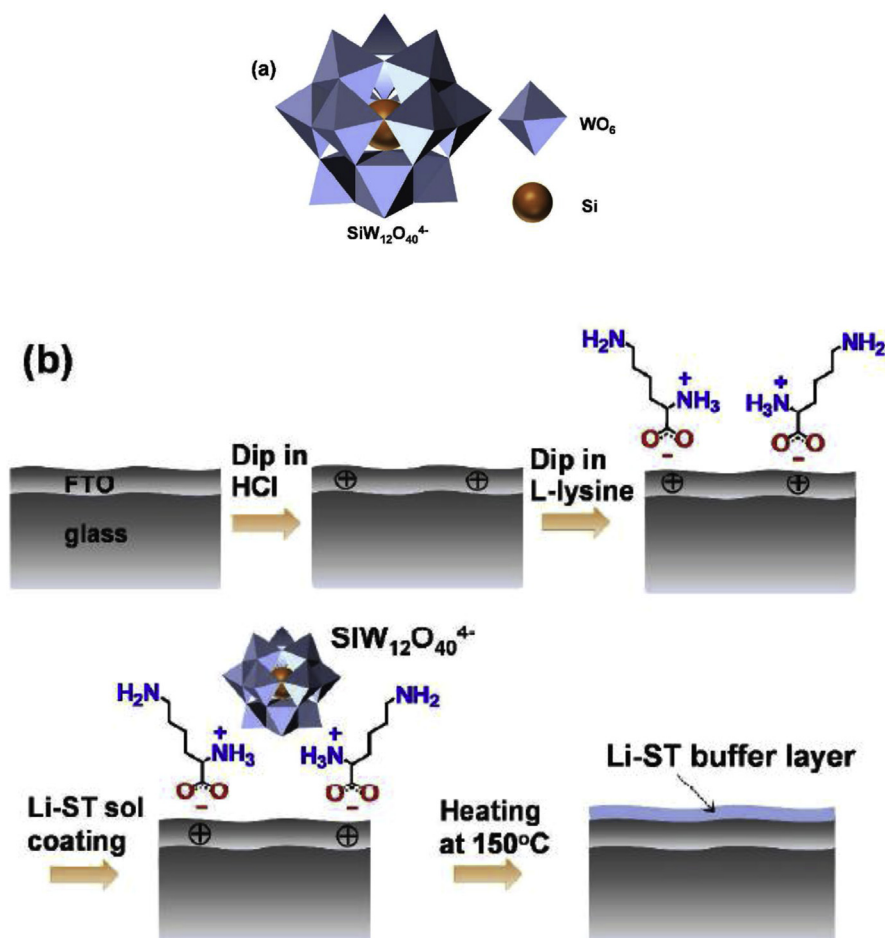
Fig. 7. (a) Crystal structure of $SiW_{12}O_{40}^{4-}$ (b) schematic diagram describing the formation of Li-ST buffer layer. (Reprinted and adapted with permission from Y.H. Choi, et al., ACS Applied Materials & Interfaces. 9 (2017) 25257−25264. Copyright (2017) American Chemical Society; Ref [133]).

layer. The CB of $SiW_{12}O_{40}^{4-}$ is (-4.55 eV) and its band gap is (3.4 eV). Therefore photo-excited electrons in the perovskite layer can be easily transferred into $SiW_{12}O_40^{4-}$ and then transported to the FTO (-4.8 V). The fabricated device by Li-ST (60 nm thickness) indicates PCE = 14.26% which is higher than that of the PSC with TiO_2 layer processed at 150 °C (TiO_2-150) (PCE = 12.27 %). In comparison with PSC with TiO_2 layer prepared at 500 °C (PSC-TiO_2-500), PSC-Li-ST-150 showed similar J_{SC} (22.16 mA cm^{-2}) and V_{OC} (0.993 mV) and lower FF (64.81 %.), showing more transporting electrons resistance through CB in the Li-ST layer than the TiO_2-500 layer. The Time-resolved photoluminescence (TR-PL) spectra measurement indicates that the Li-ST layer transports electrons from perovskite to CL more effective than the TiO_2-150, because of its more electron mobility. Thus, Li-ST is a good candidate for CL or ETL materials that can be used instead of TiO_2 in fabricating of flexible PSCs. However, it is less effective than TiO_2-500 in transporting electrons. All structures of this section are presented in Table 1. In summary,

suitable CLs include some properties such as reduced transport resistance which enhances electron extraction, good transparency in the visible region, relatively wide bandgap, appropriate conduction band (CB) level which matches CL energy levels with the perovskite layer to decrease energy loss and improve electron mobility and electron extraction between the TiO_2 and perovskite layers. Also, suitable band alignment between CL and the perovskite film increases V_{OC}. Higher electron mobility (more than TiO_2) increases the photo-generated electron transport, J_S,

Table 1. Structures and photovoltaic parameters for PSCs with alternative CLs and dopedTiO$_2$ CLs.

Structure	J_{SC} (mA.cm^{-2})	V_{OC} (V)	FF	PCE (%)	References
ITO/CdSe/CH$_3$NH$_3$PbI$_3$/Spiro-OMTAD/Ag	17.40	0.99	0.68	11.7	[44]
FTO/SnO$_2$/TiO$_2$Mesoprous/CH$_3$NH$_3$PbI$_3$/Spiro-OMTAD/Ag	20.31	0.85	0.43	7.44	[49]
FTO/SnO$_2$NC/TiO$_2$Mesoprous/CH$_3$NH$_3$PbI$_3$/Spiro-OMTAD/Ag	22.31	1.03	0.79	18.16	[50]
Glass/AZO/CH$_3$NH$_3$PbI$_3$/Spiro-OMTAD/Au	20.2	0.94	0.67	12.6	[54]
FTO/ZnO-MgO-EA$^+$/TiO$_2$Mesoprous/CH$_3$NH$_3$PbI$_3$/Spiro-OMTAD/Au	23.08	1.12	0.77	20.05	[61]
FTO/ZnO/ZnSO$_4$/TiO$_2$Mesoprous/CH$_3$NH$_3$PbI$_3$/Spiro-OMTAD/Au	19.70	1.03	0.59	12.03	[65]
FTO/TiO$_2$ QDs/TiO$_2$Mesoprous/CH$_3$NH$_3$PbI$_3$/Spiro-OMTAD/Au	22.48	1.06	0.71	16.98	[70]
FTO/TiO$_2$-CuInS$_2$-NAs/CH$_3$NH$_3$PbI$_3$/Spiro-MeOTAD/Au	17.6	0.98	0.69	11.7	[74]
ITO/CQD-TiO$_2$/CH$_3$NH$_3$PbI$_{3-X}$Cl$_x$/Spiro-MeOTAD/Au	20.4	1.09	0.78	17.5	[77]
ITO/PEDOT:PSS/CH$_3$NH$_3$PbI$_3$/HATNT/LiF/AL	21.38	1.07	0.78	18.1	[87]
ITO/TiO$_2$/PNP/CH$_3$NH$_3$PbI$_3$/Spiro-OMTAD/Ag	21.44	0.91	0.56	8.38	[90]
FTO/Nb$_2$O$_5$/AL$_2$O$_3$Mesoprous/CH$_3$NH$_3$PbI$_{3-X}$Cl$_x$/Spiro-OMTAD/Au	11.70	1.11	0.67	8.8	[91]
ITO/TiO$_2$-Cl/Cs$_{0.05}$FA$_{0.81}$MA$_{0.14}$PbI$_{2.55}$Br$_{0.45}$/Spiro-OMTAD/Au	22.3	1.19	0.81	21.4	[92]
FTO/CuI@TiO$_2$/CH$_3$NH$_3$PbI$_3$/Spiro-OMTAD/LiF/AL	23.6	1.07	0.75	19	[96]
FTO/TiO$_2$/PCBSD:GD/CH$_3$NH$_3$PbI$_3$/Spiro-OMTAD/Au	23.30	1.11	0.78	20.19	[99]
FTO/α-Fe$_2$O$_3$/α-Fe$_2$O$_3$nanoisland/MAIPbI$_3$/Spiro-OMTAD/Au	20.9	1.01	0.76	16.2	[109]
FTO/(Ti$_{1-δ}$ O$_2$)/CH$_3$NH$_3$PbI$_{3-x}$Cl$_x$/Spiro-OMTAD/Au	21.48	0.97	0.73	15.24	[120]
FTO/stacking TiO$_2$ and SnO$_2$/FA$_{0.85}$MA$_{0.15}$Pb (I$_{0.85}$Br$_{0.15}$)$_3$/P3HT/Ag	22.3	1.08	0.75	18.03	[123]
PET/ITO/ZnO-IL-BF$_4$/CH$_3$NH$_3$PbI$_3$/Spiro-OMTAD/Au	22.9	0.94	0.55	12.1	[127]
ITO/ZnO-CA/MA$_{0.6}$FA$_{0.4}$PbI$_3$/Spiro-OMeTAD/Ag	23.61	1.01	0.69	16.45	[128]
ITO/NiO$_x$/CH$_3$NH$_3$PbI$_3$/CeO$_x$/Ag	20.43	1.05	0.76	16.4	[131]
ITO/Spiro-OMeTAD/CH$_3$NH$_3$PbI$_3$/P(NDI2DT-TTCN)/Ag	22	1	0.77	17	[132]
FTO/Li-ST/CH$_3$NH$_3$PbI$_3$/Spiro-MeOTAD/Au	22.16	0.99	0.65	14.26	[133]
FTO/Nb doped-TiO$_2$/TiO$_2$Mesoprous/CH$_3$NH$_3$PbI$_3$/Spiro-OMTAD/Ag	19.07	1.02	0.73	14.21	[134]
FTO/Ta doped-TiO$_2$/TiO$_2$Mesoprous/CH$_3$NH$_3$PbI$_3$/Spiro-OMTAD/Ag	19.21	1.03	0.73	14.41	[134]
FTO/La dopedTiO$_2$/TiO$_2$Mesoprous/CH$_3$NH$_3$PbI$_3$/Spiro-OMTAD/Au	21.8	1.03	0.69	15.31	[141]
FTO/Mg dopedTiO$_2$/TiO$_2$Mesoprous/CH$_3$NH$_3$PbI$_3$/Spiro-OMTAD/Au	18.34	1.08	0.62	12.28	[145]
FTO/Sm doped TiO$_2$/CH$_3$NH$_3$PbI$_3$/Spiro-OMTAD/Ag	19.13	1.04	0.71	14.10	[146]
FTO/Nb dopedSnO$_2$/(FAPbI$_3$)$_{0.85}$(MAPbBr$_3$)$_{0.15}$/Spiro-OMTAD/Au	22.36	1.08	0.73	17.57	[147]
FTO/Ta dopedTiO$_2$/CH$_3$NH$_3$PbI$_3$/P3HT/Ag	22.1	0.85	0.42	8.17	[148]

and thus provides the fabrication of PSCs without hysteresis. CLs with higher CB level than FTO CB level displays outstanding blocking effect and high recombination blocking effect leading to higher V_{OC}.

2.2. PSCs with doped TiO_2 CL

One of the disadvantages of TiO_2 is its low electron conductivity due to low carrier density. An effective strategy to modify electronic property, is doping of TiO_2 with some elements [134]. Previous studies showed that incorporating metal ions as dopants in the TiO_2 CL can improve the device performance via some effects. In aluminum doped TiO_2, aluminum dopant passivates the electronic trap sites in TiO_2 CL. Therefore increases performance and stability in PSCs [16]. However, niobium, zinc, magnesium and cesium dopants suppress recombination process and facilitate charge extraction [135, 136, 137, 138, 139]. Yttrium doped TiO_2 improves charge extraction in PSCs [140]. J. Song et al [134] investigated the effect of or niobium (Nb) and tantalum (Ta) dopant on TiO_2 CL. 3%Ta and 3% Nb dopants could increment the electron conductivity of TiO_2. The PSCs fabricated with Ta or Nb-doped TiO_2 indicated conversion efficiency improvement from 13.66% (pure TiO_2) to 14.41% (Ta-doped TiO_2) and 14.21% (Nb-doped TiO_2). PL and EIS analyses confirmed the doped-TiO_2 could hasten electron transfer rate and diminished the recombination at TiO_2/perovskite interface. Besides, doped TiO_2 CL effectively suppressed the J-V hysteresis due to increased conductivity. Li et al. [141] prepared lanthanum (La) doped TiO_2 CL by spray pyrolysis method. Scanning electron microscopy (SEM) images reveal lanthanum dopants increment the stability of anatase phase and suppress the crystal growth in the high-temperature process [142, 143]. Thus enhance the smoothness of TiO_2 layers. La dopants improve electrons transport in TiO_2 layers, As a result, diminish electrons accumulation and reduce the recombination at TiO_2/perovskite interfaces. In addition, La dopants induce oxygen vacancies on the surface of TiO_2 grains. These oxygen vacancies trap electrons prevent charge recombination [144]. Moreover, X-ray diffraction (XRD) result reveals La-doped TiO_2 inhibits $MAPbI_3$ decomposition after 200 h aging under light irradiation, which means the improvement of photo-stability in PSCs. Wang et al. [145] reported PSCs with thin Mg-doped TiO_2 as CL. Mg-doped TiO_2 provides different effects. Mg-doped TiO_2 creates a higher CB and lower VB which match better with porous TiO_2 and perovskite energy levels and thus will diminish the energy loss via better electron transportation. Mg-doped TiO_2 provides a wider band gap with better optical transmission features and thus increases J_{SC} values. Furthermore, the downshifted VB improves holes blocking ability, reducing charge recombination and as a result, obtains a better J_{SC} and FF. A longer electron lifetime and a smaller contact resistance which confirm a low charge recombination, leading to enhancement of V_{OC} and the J_{SC}. Also, upshifted CB leads to moving electron quasi-Fermi level upward and increasing of V_{OC} and FF values. In fact, ion doping

in metal oxide is employed to obtain a suitable energy level, increment of carrier mobility and improvement of the film morphology. Xiang et al. [146], doped TiO_2 CLs with samarium (Sm), a rare earth element, by adding samarium trinitrate into the titanium precursor solution. Sm doping relatively raises the Fermi level for the CLs and decreases the charge recombination, leads to a higher V_{OC}. In addition, Sm doping reduces the energy barrier between the $CH_3NH_3PbI_3$ layer and TiO_2 CL, results in enhanced charge transport and J_{SC}. PSCs with 0.3% Sm^{3+} ion doped into TiO_2 indicate better PCE (14.10%) than nondoped devices (PCE = 12.78%). Ren et al. [147] used Nb-doped SnO_2 (Nb: SnO_2) as a CL processed by a low-temperature solution method. The amount of PCE for Nb: SnO_2 CL device improved to 17.57% in comparison to that of the single SnO_2 CL (15.13%). This improvement is related to the excellent electronic and optical features of the Nb: SnO_2 layer, such as large electron mobility (due to effective passivation of electron traps) and appropriate electrical conductivity which provides better J_{SC} and FF. Also, Nb: SnO_2 CL provides a high V_{OC} due to the reduced charge recombination. Ranjan et al. [148] reported tantalum (Ta) doping of TiO_2 CL in the structure of FTO/Ta-TiO_2/ $CH_3NH_3PbI_3$/P3HT/Ag with introducing poly-3-hexylthiophene (P3HT) as inexpensive and stable HTLs instead of expensive Spiro-OMeTAD. Tantalum (Ta) is a good element for doping in TiO_2. Because the ionic radius of Ta^{5+} ion (0.64 A°) is similar to Ti^{4+} (0.61 A°), it will appropriately substitute Ti^{4+} sites in the TiO_2 network without the producing of secondary phases. Ta doping shifts downward to Fermi level of TiO_2 and creats driving force for the electron transfer from the perovskite LUMO to the TiO_2 CB, resulting in higher J_{SC}. Furthermore, EIS measurement reveals a low R_s, related to augmented charge transport with Ta-doping, and a high R_{sh} owing to the more recombination resistance of doped films and reduced leakage paths. PSC devices with Ta doping of 3.0% indicate a 40% improvement in PCE in comparison to un-doped TiO_2. Some studies showed that most of the doping methods involve a similar way for mixing TiO_2 precursor with dopant precursor solution [136, 138, 140, 149, 150, 151, 152, 153, 154, 155, 156]. These doping methods exhibit disadvantages such as sophisticated procedures, high-temperature processing (500 °C), low control of film quality along with low efficiency, which hinders the using of doped TiO_2 film for large-scale industrial fabrication of PSCs in some substrates. To solve this problem, Liang et al. [157] suggested a one-pot solution-processed procedure with the lowest temperature (70 °C) to produce monotonous crystallized metal-doped TiO_2 film as big as 15 × 15 cm^2. A big-area metal-doped TiO_2 (W, Ta, Nb, or Sn as the dopant) is produced by doping chloride precursors of niobium (V), tin (IV), tantalum (V) to tungsten (VI). These dopants can remove deep traps of TiO_2, and also, incorporate new states near CB which increases J_{SC} (W or Sn dopant) and FF (Ta, W, or Sn dopant) via decreasing carrier recombination and increase electron transport. Ta-doped TiO_2 predominantly increases V_{OC} as a result of its higher CB in comparison to undoped TiO_2. Besides, Nb^{5+} ions result in a reduced interfacial carrier recombination and an

increased carrier transport, leading to a promising improvement in J_{SC}, V_{OC}, and FF. Doped TiO_2 PSCs show $\sim 25\%$ improvement in PCE compared with undoped PSCs. Table 1, shows structures and photovoltaic parameters for PSCs described in sections.

2.3. PSC structures without CL

The TiO_2 metal oxide is extensively employed as an ETL or CL, however, it includes high temperature for sintering process (400−500 °C) which is not appropriate for making of the flexible PSCs and increments costs for producing purposes. High temperature suppresses the using of flexible plastic substrates such as polyethylene naphthalate (PEN) and polyethylene terephthalate (PET) because they cannot tolerate high temperatures (higher than 150 °C). By eliminating CL from a device, the temperature of preparation process can be below 100 °C. Also, simple and low-cost PSCs will be created [158]. It's worth saying that the exciton binding energy in $CH_3NH_3PbI_3$ is 50 meV [159]. This means that more than 98% of the photogenerated excitons will thermally dissociate in normal operating temperatures. Thus the perovskite can act as an inorganic semiconductor thin film without a requirement for the high surface area to separate excitons. Consequently, The CL is not certainly necessary for fabrication of PSCs devices [59]. For the first time, Liu et al fabricated an effective P-PSCs without CL with a suitable PCE = 13.5%. This exhibits that the CL is not crucial for all efficient PSCs. The simplified device showed relatively higher J_{SC} and V_{OC} than those of devices with TiO_2 CL, implying more photocurrent generation and less carrier recombination [160]. In this work, the superb-quality polycrystalline perovskite layer was fabricated by two-steps spin-coating procedure, involving a substantial role in the improvement of photovoltaic parameters. However, devices with TiO_2 CL indicated a higher FF than simplified devices due to a smaller serious resistance. Liu et al. [59] fabricated a P-PSCs without CL and with a P3HT as an HTL. Device based on the ITO/ZnO/$CH_3NH_3PbI_3$/P3HT/Ag structure indicated J_{SC} = 18.8 mA/cm^2, V_{OC} = 0.94 V, FF = 66.0% and PCE = 11.7%. However, ZnO free device indicated J_{SC} = 17.2 mA/cm^2, V_{OC} = 1.01 V, FF = 66.5%, and PCE = 11.6%. In addition, the ZnO-free devices with Spiro-OMeTAD as HTL showed PCE $\sim 13.5\%$ similar to PCE = 13.7% for CL free devices with Spiro-OMeTAD as HTL. The V_{OC} is ~ 1 V for both of the P3HT and Spiro-OMeTAD devices. This exhibits the absence of a CL does not provide high charge carrier recombination. The PL spectra showed approximately complete quenching after contacting with the two hole transport materials (P3HT and Spiro-OMeTAD), but, only $\sim 40\%$ of PL quenching happened when the perovskite was connecting to either ZnO or ITO. This means that carrier extraction at the perovskite/HTL interface is much better than carrier extraction at the ZnO or ITO/perovskite interface. The high performance in the ZnO-free devices have been illustrated by highly effective hole extraction at the perovskite/HTL interface, quickly depleting the perovskite from holes and as a result suppresses

bimolecular recombination. The absence of surface recombination in the ZnO-free devices can also be owing to residual unreacted PbI_2 after the CH_3NH_3I dipping step. A residual PbI_2 layer near the transparent electrode can operate as a built-in HBL [161]. However, ZnO CL creates additional surface recombination pathways. The ZnO CL devices have a reduced contact resistance due to favorable energy level alignment of the ZnO and perovskite CB levels. However, they have a decrease in the recombination resistance, because ZnO can produce high surface energy sites that provide substantial surface recombination [162]. The reason for the loss in V_{OC} in MS-PSCs with TiO_2 as a CL was investigated by Kulkarni et al. [163]. For this propose, three different CLs were used, TiO_2 compact layer (TiO_2 CL), MgO thin layer (MgO TL) and a bilayer of TiO_2 and MgO (TiO_2-MgO bilayer). MgO TL (5nm) on FTO enhanced the V_{OC} of the TiO_2 MS-PSCs (from 0.86 (for (TiO_2 CL) to 0.98 V) in spite of having many pin holes. However, the MgO layer on 50−60 nm TiO_2 CL (TiO_2-MgO bilayer) did not indicate many variations in V_{OC} (from 0.86 to 0.9 V). These results proved that there is a logical recombination loss via trap, produced by recombination within TiO_2 itself and through back transport of electron from FTO to TiO_2, which is famous for the mirror effect. Thus, the increment of V_{OC} by the MgO TL is most probably due to blocking the recombination way at FTO/TiO_2 interface, not at TiO_2/Spiro-OMeTAD or TiO_2/perovskite interface. Furthermore, the cells with and without TiO_2 CL exhibited similar V_{OC}, which proved that the TiO_2 CL is not very necessary for inhibiting back transfer of the electron from FTO into perovskite or HTM. The schematics of feasible recombination mechanisms have been shown in Fig. 8. It indicates a MgO layer on TiO_2 CL or on FTO cannot inhibit the recombination between porous TiO_2 and HTM or perovskite. Also, charge recombination at HTM and perovskite interface will not be affected by every change in the CL. As a result, the substantial increase in V_{OC} by MgO TL compact layer is not owing to prevented back transfer from FTO to perovskite or HTM. It should be mentioned that there are trap states in TiO_2 CL [164] prepared by solution methods, which can provide trap-assisted recombination in TiO_2 [104, 165, 166, 167] and at the interface with perovskite, leading to a loss in V_{OC}. This kind of V_{OC} loss can be confirmed by the open circuit voltage decay (OCVD) measurement. Similar and fast voltage decay has been shown in TiO_2 CL and TiO_2-MgO bilayer devices whereas slow voltage decay has been shown in MgO TL device. Thus, OCVD (Fig. 9) confirms a logical loss in V_{OC} in TiO_2 CL itself. TiO_2-MgO bilayer does not indicate much increment in V_{OC}, because the recombination at FTO/TiO_2 interface is not suppressed. However, the little increment (from 0.86 to 0.9 V) is owing to passivation of superficial traps in TiO_2 CL by MgO TL. Results reveal that major reason for the loss in V_{OC} and performance in MS-PSCs with TiO_2 CL is recombination at FTO/TiO_2 interface.

Sandoval-Torrientes et al. [168] used a mixture of perovskite and chemically modified fullerenes with the various electron accepting in fabrication of CL-free cells.
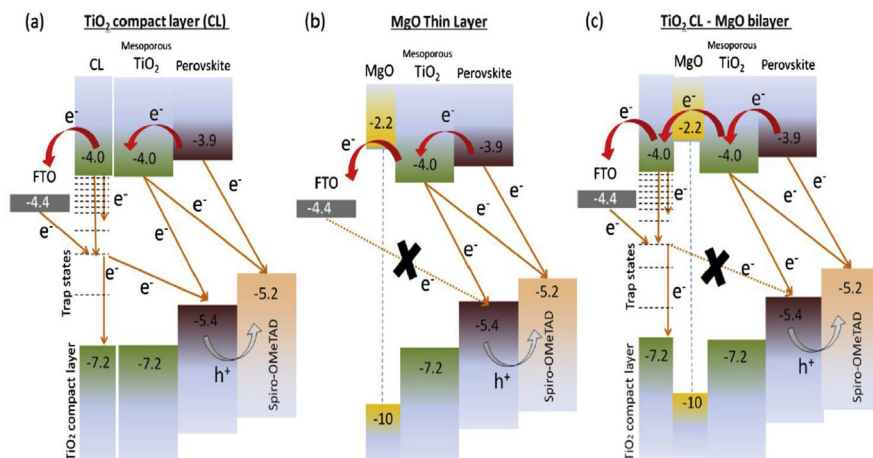
Fig. 8. Schematic diagram showing possible recombination mechanisms in TiO_2 mesostructure perovskite solar cells with (a) TiO_2 CL, (b) MgO TL and (c) TiO_2-MgO bilayer. (Adapted from Ref. [163] with permission of Elsevier).

This procedure provides simple efficient devices with high stability. The devices with various derivative fullerenes do not show differences in their photo-stability. Also, all perovskite: fullerene derivative mixture layers showed the same water contact angle, and as result the same behavior against moisture. This indicates that fullerene core itself is a major reason for stability. Amount of PCE for PSCs with mixed films (fullerene or derivatives) is further than that of the device with perovskite film without fullerene. Furthermore, solar cells based on mixture films with fullerene derivatives showed better performance than unmodified fullerene. Thus
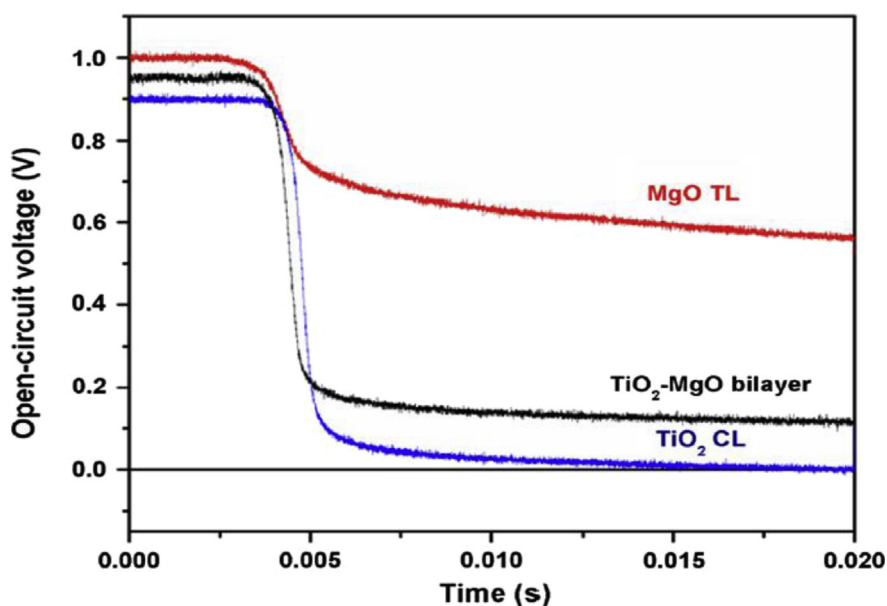

Fig. 9. Open-circuit voltage decay (OCVD) measurement of TiO_2 CL (blue trace), MgO TL (red trace) and TiO_2-MgO bilayer (black trace). (Adapted from Ref. [163] with permission of Elsevier).

chemical modified fullerenes have a useful effect. Fullerenes derivatives with less electron accepting result in an increment in the V_{OC}. Also, fullerene derivatives with a binding site for a more efficient interaction with perovskite are more beneficial. Huang et al. [169] designed a P-PSCs device without CL by Ultra-violet/ozone (UVO) treatment of FTO substrate. UVO treatment, utilizing as an atomic level surface cleaning procedure, can decrease the connection angle of the polar solvents. Consequently, the perovskite solution completely distributes on the substrate and produces a smooth film with full coverage. This improved perovskite film provides efficient charge transfer and light absorption. Thus enhances the J_{SC} and V_{OC}. Furthermore, UVO treatment can promisingly eliminate the residual organic species, increment the surface between the perovskite and the FTO layer and will reduce energy losses, enhance the FF by decreasing the R_s and increasing the R_{sh}. Therefore, FTO substrates with UVO treatment increment PCE value. In FTO substrates without UVO treatment, the perovskite film on FTO shows many pinholes and voids which cause straight contact between FTO and HTL and decrease resistance shunting paths and light absorption. Thus this device shows smaller R_{sh}, lower performance than that of the device with UVO treatment. In order to enhance the charge extraction efficiency in CL-free PSCs and reduce the hysteresis, FTO must involve a large interfacial area that can be covered by perovskite completely. Yu et al. [170] modified the surface of the FTO to a hierarchically porous surface by using electrochemical etching to improve charge extraction at the FTO/perovskite interface. By using of etched FTO (E-FTO) instead of the purchased pristine FTO (P-FTO) whose monotonous surface consists of large and sharp SnO_2 crystals, obtains a significant increase in J_{SC}. This increment is ascribed to the accelerated expulsion of unbound electrons in the perovskite due to a high interface area between the perovskite and the E-FTO (Fig. 10). A substantial performance acquired for the E-FTO-based PSC (PCE = 19.22%) which was related to high light capturing produced by a scattering effect and strong interfacial contact provided via much better surface wettability. Also, the hysteresis effect remarkably decreased in E-FTO because of fast migration of free electrons and efficient charge transfer at the E-FTO/perovskite interface which leads to fewer trapped electrons.

Hu et al. [60] used Cesium carbonate solution to modify an indium-tin-oxide (ITO) surface (ITO: Cs_2CO_3) in P-PSCs without CL. Cs_2CO_3 salt will form sub-microscale spots on the ITO substrate after solvent evaporation. The surface morphology with Cs_2CO_3 spots is similar to that of the pristine ITO surface. Thus the Cs_2CO_3 cannot form a continuous compact film on the ITO. Efficient performance (PCE = 15.1%) is attributed to generated Cs-O bonds on the ITO surface which can tailor the work function [171] and provide much better ohmic contacts between the perovskite and ITO layer [172]. Also, this device without CL has stability similar to that of TiO_2 CL device. Zhu et al. [158] introduced a CL free PSCs by a diketopyrrolopyrrole-based copolymer (P) as an HTL. This P-HTL has great hole
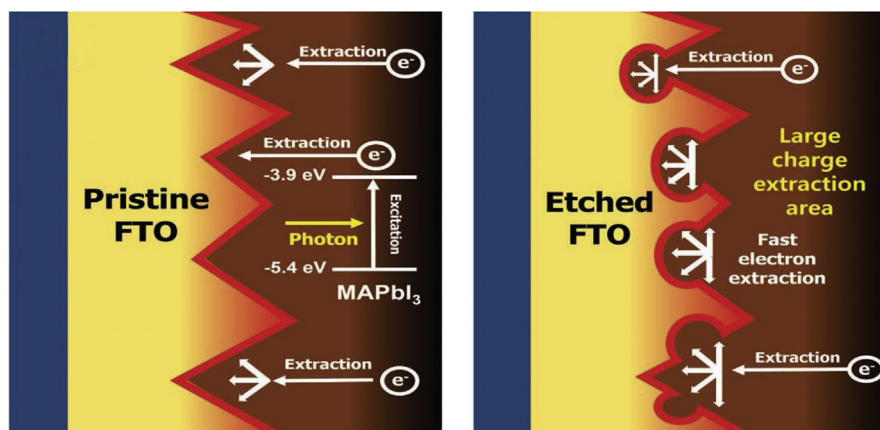
Fig. 10. Illustration of the extraction behavior of photoexcited electrons from perovskite into the FTO. The charges quickly accumulated at the interface between the E-FTO and perovskite due to the larger charge contact area of the E-FTO compared with the P-FTO. (Reprinted with permission from Ref. [170]. Copyright 2017 John Wiley & Sons, Inc).

carrier mobility, good stability, and an efficient energy level matching to perovskite. Also, its low temperature (below 100 °C) and low-cost fabrication with an excellent cell performance and simple cell structure make it useful for commercial applications. By replacing of P3HT as HTL with the P-HTL (Fig. 11), efficiency improves from 6.62% to 10.80%. The P-HTL-based device shows higher J_{SC}, because the HOMO level of P is relatively higher than the HOMO level of perovskite, leading to a low injection barrier between the perovskite layer and P-HTL. Furthermore, the slightly large energy barrier between the LUMO of P and MoO_3 can remarkably suppress electrons to diminish likely charge combination loss at the anode. As well as the mobility of P is higher than that of P3HT which is useful to hole transportation in HTL and hole collection by the anode. In spite of that the efficiency of P-based
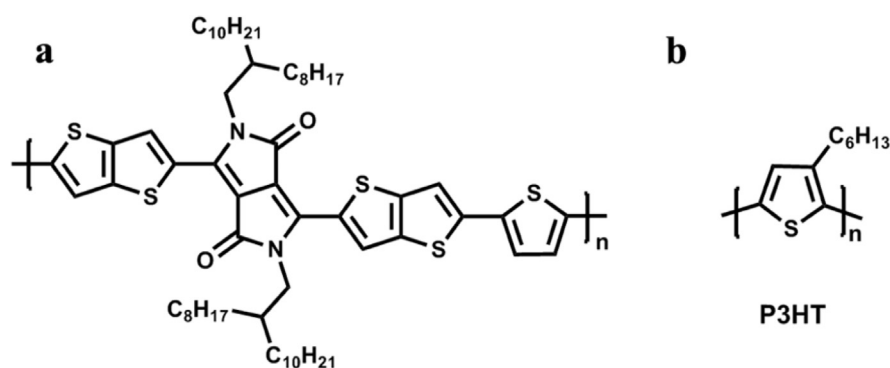

Fig. 11. (a) Molecular structure of P and (b) P3HT. (Reprinted and adapted with permission from Q. Zhu, et al., Compact layer free perovskite solar cells with a high-mobility hole-transporting layer, ACS Applied Materials & Interfaces. 8 (2016) 2652−2657. Copyright (2016) American Chemical Society; Ref [158]).

devices is lower than that of Spiro-OMeTAD-based devices, uncomplicated and low-cost synthesis of P are the best advantages for more industrial production. Yu et al. [173] fabricated highly efficient CL-free PSCs via strongly disturbing penetration of HTM into FTO layer by large grain perovskite film crystallized by solvent annealing procedure [104, 174]. The perovskite film can operate as a CL or HBL as well as an excellent sensitizer. Thus device performance can depend on grain size and thickness of perovskite layer. The results showed that over the ca. 700 nm perovskite grain size will prevent the HTM from permeating into the film due to the increased compactness and reduced grain-boundaries. As a result, a great PCE of 18.20 % obtained by using of 51 and 58 wt% based perovskite in which the perovskite can be crystallized with an ideal grain size (0.6–1 μm) and suitable coverage. By increasing of perovskite grain size, electron migration from perovskite to FTO was accelerated, because crystallinity improved and trap density in perovskite decreased. Furthermore, the HTM was more effectively deposited on the perovskite films including low surface roughness (51 and 58 wt%-based $MAPbI_3$ according to AFM). This accelerated hole-migration into the HTM. Moreover, these highly crystalline grains have intrinsic advantageous such as the long charge carrier diffusion length and lower defects. Thus, decrease non-radiative recombination and improve V_{OC} in 51 and 58 wt% based PSCs. Table 2 shows structures and photovoltaic parameters for this section.

2.4. Morphology effect

Wu et al. [16] investigated the effect of nanoscale pinholes in TiO_2 CLs on the device performance. TiO_2 CLs were fabricated by using different methods, involving atomic layer deposition (ALD), spin coating, and spray pyrolysis. Surface morphology for these TiO_2 CLs indicated that the density of nano-scale pinholes was remarkably lower in the ALD-based TiO_2 CL, but TiO_2 CLs with spin coating

Table 2. Structures and photovoltaic parameters in PSCs without CLs.

Structure	J_{SC} (mA.cm^{-2})	V_{OC} (V)	FF	PCE (%)	References
ITO/CH$_3$NH$_3$PbI$_3$/P3HT/Ag	17.2	1.01	0.66	11.7	[59]
FTO/MgOTL/TiO$_2$ Mesoprous/CH$_3$NH$_3$PbI$_3$/ Spiro-OMTAD/Au	16.65	0.99	0.53	8.89	[163]
FTO/CH$_3$NH$_3$PbI$_3$:fullerene derivative/ Spiro-OMeTAD/Au	16.1	1.06	0.74	12.7	[168]
FTO/CH$_3$NH$_3$PbI$_{3-x}$Cl$_x$/Spiro-OMeTAD/Ag	17.1	0.97	0.62	10.67	[169]
FTO/CH$_3$NH$_3$PbI$_3$/Spiro-OMTAD/Au	22.81	1.12	0.75	19.22	[170]
ITO/Cs$_2$CO$_3$/CH$_3$NH$_3$PbI$_3$/Spiro-OMTAD/Au	19.1	1.05	0.72	14.4	[60]
ITO/CH$_3$NH$_3$PbI$_3$/P/MoO$_3$/Ag	18.47	0.88	0.67	10.80	[158]
FTO/CH$_3$NH$_3$PbI$_3$/Spiro-OMTAD/Au	21.45	1.13	0.75	18.2	[173]

and spray pyrolysis methods showed a relatively high density of nano-scale pin-holes, leading to increase charge recombination and decrease V_{OC} compared with an ALD-based TiO_2 CL device. Devices without a CL provided low performance with low J_{SC}, V_{OC}, and FF values. This is ascribed to the significant contact between the FTO and perovskite and/or HTM. Conversely, after adding a CL, the device performance improved. This proves the importance of the CL in the device. The best performance with best parameters was for ALD based TiO_2 CL. The ALD-TiO_2-based cell exhibited higher R_{sh} than the other devices, providing predominant suppression of charge recombination and leading to its higher V_{OC}. The R_s of the ALD-TiO_2-based cell was less than those of the spin-coat and pyrolysis TiO_2-based devices. The higher R_{sh} and lower R_s provide a larger FF. Also, J_{SC} of the ALD-TiO_2 CL device was higher than those of other devices. Because the absorption spectra of perovskite films for different TiO_2 CLs are almost similar, the improved J_{SC} may be related to a smaller number of dead points provided by pinholes. Studies have revealed that perovskite crystallization depends on the surface features of the substrates. Obviously in $CH_3NH_3PbI_3$ perovskite film, when the substrates covered with ammonium or amino group, smooth and high crystalline perovskite films would grow. Zuo et al. [175] demonstrated a method to modify the substrate with self-assembling monolayers of 3- Aminopropanoic acid (C_3-SAM) onto ZnO CL. This improves the morphology of $CH_3NH_3PbI_3$ perovskite film via the enhanced wetting between the ZnO substrate and perovskite. The AFM and SEM images reveal the extended crystalline domains in the lateral orientation with the morphology change of perovskite film from rod-like to plate-like via deposition of C_3-SAM on ZnO. It is ascribed to the enhanced substrate miscibility with perovskite, where the amino group changes into ammonium via hydrogen ion exchanging and adds into the crystalline structure of perovskite. The using of C_3-SAM can improve the energy level matching and electronic coupling between the ZnO and perovskite which enhances the carrier extraction. Improvement of interfacial energy level alignment can be related to the formation of a permanent dipole moment (Fig. 12). An improvement in device performance showed the increment of PCE from 11.96% to 15.67% via deposition of C_3-SAM on CL. Yella et al. [176] deposited a nanocrystalline TiO_2 (with rutile phase) as a CL ($\sim$25 nm) on FTO substrate by hydrolysis of $TiCl_4$ (200 mM) at 70 °C. The rutile nanoparticles produced by chemical bath deposition can adjoin greatly to the FTO, thus more calcination or sintering process is not necessary for the formation of the TiO_2 CL. The formation of rutile phase in low temperature instead of anatase phase (as the stable low-temperature TiO_2 phase) is attributed to the using of a $TiCl_4$ precursor which can create rutile nanoparticles by hydrolysis, and also FTO substrate which involves a rutile crystal structure for induction of epitaxial growth of rutile nanoparticles. The rutile TiO_2 cell provides much better performance (PCE = 13.03%) than an anatase TiO_2 produced by spin coating of $TiCl_4$ at high temperature (450 °C) (PCE = 3.7%). This was explained by the formation of an intrinsic contact between the nanocrystalline rutile TiO_2
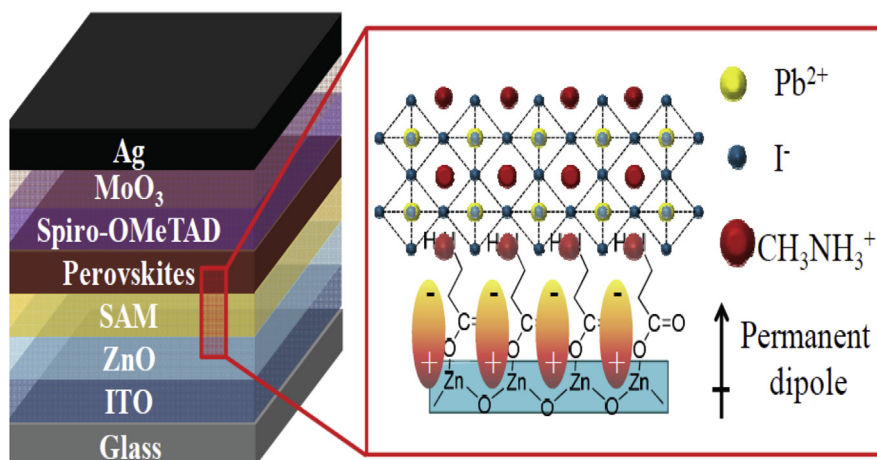
Fig. 12. Schematic diagram of perovskite solar cell device structure, SAM induced permanent dipole formation, and involvement of the SAM in the crystalline structure of perovskite crystals. (Reprinted and adapted with permission from L. Zuo, et al., Journal of the American Chemical Society. 137 (2015) 2674−2679. Copyright (2015) American Chemical Society; Ref [175]).

and the perovskite layer in a huge interfacial area which enhances extracting photo-generated electrons much better than the anatase film. Thus, high efficiency with a remarkably high V_{OC} (1110 mV) will obtain. Ren et al. reported that the PSCs with amorphous TiO_2 CLs exhibit better performance than PSCs based on annealed anatase TiO_2 CLs. A room temperature process was used for fabrication of TiO_2 CL in PSCs by sputtering amorphous TiO_2. Amorphous TiO_2 is extensively transparent over the solar spectrum and enhances electron extraction ability and decreases interface transfer resistance. Besides, its Fermi energy level can coincide with the LUMO of the perovskite in comparison with anatase TiO_2 [177]. The outstanding wettability of amorphous TiO_2 against perovskite solution is useful for enhancing the contact between TiO_2 and perovskite layer. However, amorphous TiO_2 involves some disadvantages comparing to anatase TiO_2 such as higher electron traps density, slower electron transport, and slightly weaker transmittance which have an important role in the V_{OC} of P-PSCs [178]. The performance of PSCs depends on the crystallinity of TiO_2. Huang et al. [179] investigated TiO_2 films with various crystallinities by DC magnetron sputtering without any post thermal treatments and at room temperature. The inserted crystallized grains can improve the general crystallinity and reduce the trap state density in film and somewhat increment the transmittance. Thus, will reduce the structural disorder and improve the electron transport efficiency. Partly crystalized TiO_2 (PC-TiO_2 CL) with 26.3% crystallinity indicated the best photovoltaic performance comparing with amorphous TiO_2 (am-TiO_2 CL), anatase TiO_2 (an-TiO_2 CL). Maximum J_{SC} in PC-TiO_2 is related to a smoother surface which confirmed good quality of perovskite film, smaller interface resistance, and lower trap states density. Thus, superior electrons extraction is provided. Also, oxygen vacancies for hole conducting diminished which reduced the carrier transport loss and

improved visible light transmittance as well as harvesting ability [180]. PC-TiO$_2$ has maximum FF owing to increase charge extraction and decrease carrier transport loss. The V$_{OC}$ was determined by the difference between the CB position of CL and valence band position of HTL (energy band diagram shown in Fig. 13). Therefore the increase of V$_{OC}$ was expected for an-TiO$_2$. The PCE of the device based on PC-TiO$_2$ CL (15.76%) was better than that based on am-TiO$_2$ CL (13.3%) and an-TiO$_2$ CL (12.9%). A low temperature (150 °C) processed PSCs was fabricated by Kogo et al. [181] with an ultrathin (8 nm) amorphous TiO$_x$ CL along with brookite TiO$_2$ as a CL. Hydrophilic surface of brookite TiO$_2$ nanoparticles enriched with hydroxyl groups, providing an inter-particle connection via dehydration reaction at low temperature (150 °C) and thus, creates a mesoporous layer. This brookite mesoporous layer operates as well as traditional anatase TiO$_2$ mesoporous prepared at 500 °C. This PSC with TiO$_x$/brookite TiO$_2$ presents high efficiency up to 21.6% along with high V$_{OC}$ and FF up to 1.18 V and 0.83, respectively. Su et al. [182] reported a mossy structure TiO$_2$ as CL in MS-PSCs by electrodeposition (ED) method. This three-dimensional interfacial contact provides a full covered ultrathin morphology and also a firmly anchoring effect for the TiO$_2$ layer to reduce the contact resistance and enhance efficient electron transport [183]. Thus, lower ohmic resistance (lower R$_s$), higher R$_{sh}$ and higher FF will be provided in this ED method comparing with other methods (dip coating (DC), spin coating (SC), and spray pyrolysis (SP)). The hole-blocking ability for various CLs (prepared with various methods) was examined by cyclic voltammetry (CV) of the FTO layer coated by them (Fig. 14). In CV voltammograms, larger values of ΔE_p means slow electron transportation kinetics. The cathodic peak current (I$_{PC}$) of the CV is related to the reacting area of the electrode (A) according to the Randles−Sevcik equation (I$_P$ = k$\times$n$^{3/2}$ $\times$A$\times$ c$\times$D$^{1/2}$ $\times$ υ$^{1/2}$) when other parameters in a reaction are constant. (n) shows the number of electrons transferred in the redox couple, (υ) indicates the scan rate, and (D) shows the diffusion coefficient. Covering the FTO surface with a CL decreases the reaction area for the redox reaction, resulting in a reduced I$_P$. Thus, the ratio of (I$_{PC}$ (CL)/I$_{PC}$ (FTO)) can be employed as an index to confirm the surface coverage by a CL. ED-CL indicated the highest performance comparing
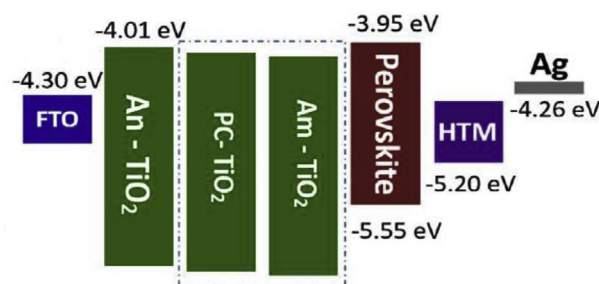

Fig. 13. Energy band diagram of the PSC. (Adapted from Ref. [179] with permission of Elsevier).
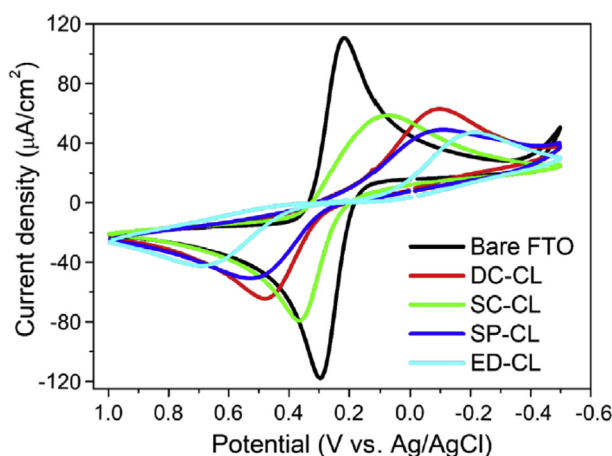
Fig. 14. CV waves of bare FTO, DC-CL, SC-CL, SP-CL, and ED-CL. The values were recorded at a scan rate of 50 mVs^{-1} in 0.5mM $K_4Fe(CN)_6$ and $K_3Fe(CN)_6$ with 0.5M KCl aqueous solution. (Reprinted with permission from Ref. [182]. Copyright 2018 John Wiley & Sons, Inc).

with other CLs, according to the largest ΔE_P and smallest I_{PC} (CL)/I_{PC} (FTO) for ED-CL. The CV waves of DC-CL and SC-CL indicated a Nernstian shape, proving charge transfer proceeded by pinholes. However, the CV waves for SP-CL and ED-CL were considerably broadened from the ideal Nernstian shape, confirming that charge transfer happened by a tunneling effect [184]. Field emission scanning electron microscopy (FESEM) images for SPCL and ED-CL indicate good surface coverage, confirming charge transfer in the film via electron tunneling. Also, FESEM images show pinholes in SC-CL and unsuitable surface coverage in DC-CL. The tendency of J_{SC}, V_{OC}, and FF indicated the order of ED-CL > SP-CL > SC-CL > DC-CL. Because the perovskite layer was fabricated by the similar process, therefore, J_{SC} can affect the charge extraction and collection ability of the TiO_2 scaffold and CL. In addition, ED-CL showed the lowest hysteresis among the CLs because of the highest charge extraction ability and lowest R_s. The PCE improved from 10.71 for CL-free PSC to 15.48% for ED-CL PSC which was according to improve FF (from 0.619 to 0.748) and J_{SC} (from 17.33 to 19.86 mA. cm^{-2}). Results show that the existence of a CL can improve J_{SC}, but a CL will have a more important effect on FF than J_{SC} in MS-PSC. Table 3 shows photovoltaic parameters.

Wang et al. [185] proposed a CL-assisted nucleation and growth approach to fabricate P-PSCs. This is a method for the crystal engineering of perovskite materials by using of CPTA (C_{60} pyrrolidine tris-acid) as a CL which can produce a nucleation matrix for the coordination of PbI_2 (CPTA: PbI_2). Thus, provides a controllable nucleation density with a high electron transport feature. In fact, octahedral coordination structure was formed via chelation of Pb^{2+} with carboxylic acid groups of CPTA, leading to heterogeneous nucleation center with a remarkable decrease in

Table 3. Photovoltaic parameter. (Reprinted with permission from Ref. 182. Copyright 2018 John Wiley & Sons, Inc).

Type of CL	J_{SC} (mA/cm^2)	V_{OC} (mV)	FF	PCE (%)
CL-Free	17.33	0.998	0.619	10.71
DC-CL	19.46	1.059	0.618	12.71
SC-CL	19.06	1.060	0.675	13.64
SP-CL	19.76	1.048	0.695	14.39
ED-CL	19.86	1.051	0.748	15.48

configurational entropy loss [186] and nucleation barrier, therefore accelerates tetragonal perovskite phase formation. Furthermore, the carboxylic acids of CPTA are attached to OH groups on the ZnO CL and operate as a chemical protective interfacial between ZnO and the perovskite. These OH groups on the ZnO, as Lewis acid sites, can deprotonate methylammonium ion (MA^+) and then decompose perovskite crystals into a yellow film. A 0.30 molar ratio of PbI_2 to CPTA was employed to improve the crystallization of perovskite, resulting in a PCE of 20.20% along with a $V_{OC} = 1.114$ V, $J_{SC} = 22.36$ mA cm^{-2}, FF = 81.13%, and less hysteresis effect. The slight increase in the FF is attributed to decrease in defect states and energy traps and increase in the electron quality of the perovskite films. Deng et al. [187] demonstrated room temperature processing for fabrication of TiO_2 CL by using of titanium (IV) isopropoxide in isopropanol Ti(OiPr)$_4$. Traditional precursor solution, titanium diisopropoxide bis(acetylacetonate) in butanol, needs to high temperature (500 °C) for pyrolysis and forming titania CL because the acetylacetone groups in traditional precursor have slower hydrolysis [188]. However, Ti(OiPr)$_4$ can easily form a titania layer at room temperature. Raman spectroscopy shows that TiO_2 fabricated by Ti(OiPr)$_4$ is amorphous (there are no obvious peaks). But, TiO_2 fabricated by traditional precursor shows peaks at 145, 398, 516 and 640 cm^{-1} for an anatase phase [189]. TiO_2 CL by using of Ti(OiPr)$_4$ is amorphous with organic residues, however, its electrical and optical properties are relatively similar to the TiO_2 CL fabricated at high temperature. Flexible PSCs fabricated by this the room temperature process shows a PCE = 14.3% with outstanding mechanical durability and stability. Photovoltaic parameters and structures for this section were summarized in Table 4.

2.5. CLs with different fabrication methods

Many techniques have been introduced to fabricate CLs such as spin coating [190], spray pyrolysis [191], atomic layer deposition [16], electrodeposition [192], thermal oxidation [193], etc. Among them, spin coating (SC) and spray pyrolysis (SP) are two solution methods to the fabrication of CLs [39, 194, 195] which the quality of CLs are intensively depended on process parameters. Also, there are not controllability to form continuous films in these methods and proper coverage usually increases the

Table 4. Structures and photovoltaic parameters for CLs with different morphologies.

Structure	J_{SC} (mA.cm^{-2})	V_{OC} (V)	FF	PCE (%)	References
FTO/TiO$_2$/TiO$_2$ Mesoporous/CH$_3$NH$_3$PbI$_3$/ Spiro-OMTAD/Au	18.74	0.93	0.72	12.56	[16]
ITO/ZnO/C$_3$-SAM/CH$_3$NH$_3$PbI$_3$/Spiro- OMTAD/MoO$_3$/Ag	22.51	1.07	0.65	14.25	[175]
FTO/TiO$_2$/CH$_3$NH$_3$PbI$_3$/Spiro-OMTAD/Au	17.41	1.11	0.66	13.03	[176]
FTO/TiO$_2$/CH$_3$NH$_3$PbI$_3$/Spiro-OMTAD/Ag (am-TiO$_2$)	20.99	0.99	0.66	13.30	[179]
(Pc-TiO$_2$)	23.13	1.036	0.68	15.76	
(An-TiO$_2$)	19.64	1.05	0.55	12.19	
ITO/TiO$_2$/Brookit TiO$_2$/CH$_3$NH$_3$PbI$_3$/ Spiro- OMTAD/Au	22.60	1.18	0.83	21.6	[181]
FTO/TiO$_2$/TiO$_2$ Mesoporous/CH$_3$NH$_3$PbI$_3$/ Spiro-OMTAD/Au	19.89	1.01	0.75	15.48	[182]
ITO/ZnO/CPTA:PbI$_2$/CH$_3$NH$_3$PbI$_3$ /Spiro-OMTAD/Au	22.36	1.11	0.81	20.20	[185]
ITO/TiO$_2$/CH$_3$NH$_3$PbI$_3$/Spiro-OMTAD/Ag	20.04	1.00	0.71	14.3	[187]

film thicknesswhich increments the internal resistance of the cell. However, Electrodeposition (ED) is an unsophisticated, inexpensive, and scalable technique to achieve a compact and uniform surface cover without the using of a high temperature or vacuum process Furthermore, morphology and film thickness will be simply controlled by changing of the deposition conditions in ED. Su et al. [192] employed the ED method for fabrication of an ultrathin TiO$_2$ CL (ED CL) which presents appropriate surface coverage compared with CL fabricated by the SC method (SC CL). An ED CL can decrease interfacial recombination, improve blocking ability and enhance the photovoltaic properties of the PSC compared with an SC CL. Therefore ED CL indicates better performance (PCE = 13.6%) than SC CL (PCE = 10.42), which is related to increase J_{SC} and FF in ED CL. The high J_{SC} is ascribed to a low recombination, high charge collection ability. Also, high FF is due to low ohmic resistance in thin and compact TiO$_2$ CL. Most of the applied methods need to high temperature (500 °C) for sintering. Thus, restrict the using of substrates. Rajmohan et al. [196] used reactive magnetron sputtering for fabrication of crystalline anatase TiO$_2$ as a CL at a low temperature (150 °C). This low temperature process will develop the using of cheaper and flexible polymer substrates. Polymer substrates provide light and flexible devices which were used in power generating textiles and flexible electronics [197]. Before deposition of the TiO$_2$ CL in this work, plasma treatment FTO substrate with argon and oxygen was carried out for removing the surface organic pollutants and the improving the coherence between the TiO$_2$ film and the FTO substrate.

PSC with the plasma treatmented FTO indicated better performance than the untreated FTO. A high performance (PCE = 8.7%) acquired with a 76 nm thick CL at 60 min reactively sputtered. The increment in the V_{OC} is ascribed to the decrease in recombination due to enhanced electron transport at the plasma treated FTO and TiO$_2$ interface. Du et al. [198] applied a facile and low-temperature anodic oxidation (AO) procedure for fabrication of homogeneous and compact titanium dioxide film. The AO has been utilized to fabricate metallic oxide nanotube and a compact metallic oxide layer [199, 200]. AO is useful for fabrication of TiO$_2$ at low temperature (below 120 °C), thus enhances the development of flexible PSCs. In this method, the thickness of film and morphology can be adjusted by oxidation voltage and electrolyte component. In addition, AO is an environmentally friendly method. Ti-coated ITO glass was placed on the anode section, a TiO$_x$ film was slowly formed with the AO processing. Finally, AO-TiO$_2$ film acquired by sintering TiO$_x$ at 120 °C for 40 min. Ethylene electrolyte along with the application of 30 V oxidation voltage was suitable for providing desirable AO-TiO$_2$ morphology with an optimum thickness between 50-60 nm. PCE over 13.47% obtained which included higher V_{OC} and larger FF compare with traditional high temperature processed TiO$_2$ CL. The increment of device performance is related to more efficient electron transfer from perovskite toward AO-TiO$_2$ layer and the decreased R_s. Another environmentally friendly method was introduced by Wang et al. [201]. It was an easy and a low-cost homogeneous precipitation method for deposition of CdS film in urea solution with a low temperature (90 °C). A uniform thin CdS film with proper morphology was achieved by a proper concentration of urea (1.5 M) which provided a higher interfacial area and electron mobility. This high electron mobility is useful for electron transportation in the CL and decrease of R_S in cell. Also, uniform CdS film operates as a good scaffold for the organization of the dense crystalline perovskite layer and a superior junction between CdS and perovskite layer. Although this method shows low PCE, it is environmentally friendly and can be used for large-scale device fabrication. Traditional methods used for the preparation of TiO$_2$ CL such as spin coating [40], electrochemical deposition [202] spray pyrolysis [38, 39], and thermal oxidation [203, 204] need to thermal post-treatment at high temperature (>450 °C) to provide suitable electronic contact. Such high temperatures not only lead to increment cost and lack of application in flexible substrates but also increment the presence of pinholes in the TiO$_2$ CLs [57] which reduces PSCs performance [162]. In addition, these methods are not suitable for precise controlling of CL thickness. Shalan et al. [205] fabricated a TiO$_2$ CL via atomic-layer deposition (ALD) without any thermal post-treatment at high temperature. The ALD methods indicate advantages such as acting at a low temperature, exact controlling of thickness and providing uniform film [206, 207, 208]. Also, ALD achieves a homogeneous pinhole-free film of TiO$_2$, because it involves oxidizing precursors at two separate stages without any sintering step after the deposition of the CL. The PCE = 15.03% acquired for optimum thickness of 200 nm for TiO$_2$ in MS-PSCs. ALD method shows the fabrication of PSCs with acceptable

reproducibility and a stability over a period of 500 h. In fact, the ALD method is a beneficial procedure to depose ultra-thin films in nanoscale. PSCs with conversion efficiency up to 19% were achieved via fabrication of high flatness and compactness TiO_2 by ALD [16]. Despite all these benefits, ALD is an expensive method and needs to ultra-high vacuum which restricts large-scale fabricating and commercialization of PSCs. A simple and inexpensive solution-processing method was reported by Anaraki et al. [209]. A P-PSC with great efficiency (PCE = 20.8%) was fabricated by SnO_2 CL. Spin coating (SC) of a $SnCl_4$ precursor solution in combination with a post-treatment chemical bath deposition (SC-CBD) was used for the preparation of SnO_2 CL and then the function of this device is compared to those made with other deposition methods, Spin coating (SC) and ALD method. Devices with solution-processed SnO_2 layers (SC and SC-CBD) indicate an enhanced FF about 80%, but ALD PSCs indicate lower FFs compared to SC and SC-CBD, which is related to high R_s as a result of a further resistive and very homogenous SnO_2 layer in ALD PSCs. Higher V_{OC} (1.214 V) acquires for SC-CBD similar to ALD (1.2 V), whereas lower V_{OC} is for SC method. Thus, the using of the post-treatment by CBD is beneficial to obtaining high V_{OC}. Compare to other deposition methods (ADL, SC), this combined SC-CBD deposition method presents proper photovoltaic parameters and the best efficiencies along with improved hysteresis and great long-term photo-stability. Ke et al. [193] obtained a thin and very dense TiO_2 film by thermal oxidation of Ti films which coated on FTO layer by radio frequency (RF) magnetron sputtering of a Ti target. The thickness of the Ti film can be controlled by the time of sputtering. A 400 nm TiO_2 porous film was spin coated on the Ti film. Then, the TiO_2 CL and the TiO_2 porous layer were sintered in one-step at 500 °C. Duration of sintering, Ti film can be oxidized to a compact TiO_2 and transparent film. The optimum thickness of the TiO_2 CL via thermal oxidation is 15 nm (thinner than the spin coating method with two-step sintering process). Comparing to the two-step sintering process, this one-step sintering process results in a lower dark current density with a lower interface resistance between the TiO_2 CL and the porous TiO_2 layer and also a lower R_s and a higher recombination resistance. Therefore, PSCs with thermal oxidation show a higher J_{SC} and FF, which improve the PCE of the device from 13.47% for spin coating method to 15.07% for thermal oxidation method. Another thermal oxidation method for fabrication of the TiO_2 CL and scaffold porous layer simultaneously via one-step sintering process [72] was introduced by Zhao et al. However, it was expensive and sophisticated which was not appropriate for large area device preparation. Among various methods such as spray pyrolysis, atomic layer deposition, electrochemical deposition, thermal oxidation, and spin coating, the dip coating method suggests many advantages such as solution processing, much better scale-up probability, and less waste. Hong et al. [210] used a simple and low-cost dip-coating method to deposit highly TiO_2 CL. It does not need to expensive and complicated equipment and can be used for large area device fabrication. A volumetric ratio (1:13) of an ethanolic solution of Ti precursor with optimum thickness (55 nm) of TiO_2 CL indicated

PCE (12.82%), higher than that of a spin-coating method. There are several reports that use dip coating method for fabrication of TiO_2 CL in PSCs [210, 211]. However, only TiO_2 CLs with $40-130$ nm thickness were reported which showed that device performance dropped with increasing of layer thickness due to more charge trapping and later recombination. Ledezma et al. [212] used a low-cost dip coating method for fabrication of uniform ultra-thin ($5-50$ nm) TiO_2 CL by using of titanium tetrachloride ($TiCl_4$) as a precursor as an alternative for titanium isopropoxide. $TiCl_4$ precursor produces denser film than other precursors, decreases pinholes and increases the performance [213]. Also, shows less hysteresis and more stability. A TiO_2 layer with a thickness up to $20-30$ nm improved PCE further than 50% from 5.5% (without TiO_2) to $\sim 8.6\%$ ($20-30$ nm TiO_2) due to enhanced J_{SC}. Devices without or with very thin TiO_2 CLs exhibit an "s-shaped" characteristic in the negative voltage range of J-V curves which is related to collected negative ions at the electron-extracting interface. X-ray photoelectron spectroscopy (XPS) measurements prove that the s-shape characteristic is correlated to pinholes in TiO_2 CL while it is too thin. Obviously, this effect will occur by an unsuitable interface which involves trapped ions between the perovskite and the exposed FTO surface. Nonetheless, when inserting the TiO_2 CL, the surface coverage improves gradually. Thus, the electron collection increases and the s-shape disappears. Another method to the fabrication of CLs is a thermal evaporation method. The first thermal evaporated-deposited PSCs with proper efficiency (PCE = 15%) involved high temperature processed TiO_2 CL [214]. Compared with a spin-coating method, in thermal evaporation method materials can be uniformly covered on substrates in particular with an ultrathin layer. Zhao et al. [215] fabricated an efficient metal oxide-free and annealing-free P-PSCs by thermal evaporation of both the fullerene C_{60} as the ETL and the perovskite as an absorber. The high performance (PCE = 14.9%.) obtained via an ultrathin C_{60} layer (5.5 nm) which efficiently transfers the electrons and blocks the holes due to the desired energy level alignment between C_{60} and FTO electrodes. The C_{60} layer not only operates as an electron-selective contact and HBL but also it provides a proper contact with the perovskite layer and improves the crystallinity of film. The devices with C_{60} interfacial layers show high FF and high performance due to slow recombination and fast electron extraction at the interface between C_{60} and perovskite layers. A low-temperature solution-process which simplify manufacturing processes is useful for roll-to-roll industrial mass production on flexible substrates. Zhang et al. [216] reported a simple and low-temperature solution-processed ligand-exchange procedure for fabricating of high-quality TiO_2 nanocrystals (NCs) in P-PSCs. Generally, oleic acid (OA) molecules were employed as surface ligands for fabrication of crystalline and uniform TiO_2 nanocrystals. The OA is a long hydrocarbon molecule which involves an important role in the synthesis of TiO_2 NCs with high quality and in stabilizing of TiO_2 NCs in nonpolar and hydrophobic solvents [217]. However, without decomposition process in high temperature, OA molecules operate as an insulating barrier leading to reduce electron transportation in TiO_2 CLs. However, these OA

molecules can be exchanged with BF^{4-} anions in the $NOBF_4$ reagent. Ligand-exchange can separate insulating AO ligands from TiO_2 surfaces and produce high-quality TiO_2 at low temperature (150 °C). This TiO_2 CL fabricated by ligand-exchange (OA-free TiO_2 NCs) involves some advantages such as better conductivity, superior electron transportation, higher R_{sh} and lower R_s. Thus, OA-free TiO_2 CLs devices improve photovoltaic performance from PCE = 12.7% (for OA-capped TiO_2) to PCE = 19.03% along with low hysteresis and superb reproducibility. In order to decrease the reaction time over traditional non-aqueous sol−gel synthesis and a better control of the temperature, pressure and reaction time, microwaves procedure was used which improves efficiency and reproducibility [218]. Furthermore, this method indicates high scalability of the film deposition process. Abulikemu et al. [219] employed a microwave-assisted non-aqueous sol−gel (MWNASG) method to the preparation of SnO_2 nanoparticles for fabrication of SnO_2 CLs. These nanoparticles show ultra-small size and crystallinity to form a compact film. Also, a large band gap for these nanoparticles shows low defect concentration which is one of the advantages MWNASG method. SnO_2 nanocrystal-based CLs show high transparency which increases J_{SC} (21.2 mA cm^{-2}) compared to its TiO_2-based device (15.8 mA cm^{-2}). In addition to fabrication methods, some the factors can be effective during the processes. Vivo et al. [213] compared three different precursor solutions for the preparation of CL by a spin coating method. Titanium tetrachloride dissolved in water (denoted as c-$TiCl_4$), as well as titanium isopropoxide (TTIP), dissolved in absolute ethanol (c-EtOH) or in anhydrous isopropanol solution (c-IPA). $TiCl_4$ is an inexpensive precursor which does not require expensive anhydrous solvents and can be prepared in water. The prepared films by the TTIP precursor were thinner (~45 nm) than the ones produced from the c-$TiCl_4$ precursor solution (~60 nm). The optimal film thickness for a spin-coated c-TiO_2 layer with no pinholes was between 20 and 100 nm [220, 221], all thicknesses were in this range. The c-$TiCl_4$ film shows larger anatase crystallites (~25 nm) due to the faster hydrolysis of the aqueous c-$TiCl_4$ precursor solution. In comparison to anhydrous c-EtOH and c-IPA solutions. R_{sh} for c-EtOH and c-$TiCl_4$ cells are similar and relatively higher than R_{sh} for c-IPA cells. This is confirmed by the relatively higher V_{OC} values of the c-EtOH and c-$TiCl_4$ cells (0.95 and 0.93 V respectively) than V_{OC} values of c-IPA cells (0.90 V), which results from the reduced charge recombination [16]. The highest FF values obtained for c-EtOH and c-$TiCl_4$ cells, which were according to lower R_S for them. These different CLs do not remarkably influence PSCs efficiency due to the similar titania layers fabrication. However, c-$TiCl_4$ formed CL with bigger crystals which proposes fewer grain boundaries operating as trap states in the c-$TiCl_4$ film. Thus the hysteresis effect reduces for c-$TiCl_4$ devices. Also, the c-$TiCl_4$ devices show the slowest degradation in ambient. But, TTIP devices show the fast degradation. Because TTIP devices possess smaller crystallite sizes with a higher surface area, thus their structures change quickly to diminish their surface energies [222]. Li et al. [223] investigated the effect of precursor concentrations and deposition cycles

on the performance of PSC. The volume ratios of TiO_2 precursor (titanium diisopropoxide bis(acetylacetonate) in 2-propanol) were varied from 1 to 0.25 along with various cycle numbers from one to four for depositing TiO_2 CLs (Table 5). Three-layer CLs involves a smoother surface with higher compactness than other CLs. Diluted precursor produced the same thickness of TiO_2 CLs. By diluting the precursor solution and increasing deposition cycles, can suppress pinholes in TiO_2 CLs. As a result, the TiO_2 CLs obtained by multi-cycle deposition facilitate electron transport, improve PSC performance (PCE = 14.04% for 3 cycles) (Table 6). The hysteresis for three deposition cycles was negligible due to a good quality of TiO_2 film and more rapid charge transfer via TiO_2. EIS analyses showed that charge recombination reduced remarkably and the electron transport improved after appropriate cycles of spin-coating.

Starowicz1et al. [224] compared PSCs with CL fabricated by aged titanium sol-gel with those of fresh sol-gel. Sol-gel is an inexpensive, easy procedure with high repeatability. PSCs with TiO_2 CL from the fresh sol (deposit 1 hour after preparation) and from aged sol (the milky one stored for at least 1 month) indicated the considerable difference in their performance. Devices prepared by aged sol showed

Table 5. Detailed experimental parameters of TiO_2 CLs spin-coated on FTO substrates. (Adapted from Ref. [223] by permission from Springer Nature, Journal of Materials Science: Materials in Electronics, Improved performance of perovskite solar cells by optimizing deposition parameters of TiO_2 compact layers, S. Li, et al., Copyright (2017)).

Deposition times	Concentration of TiO_2 precursor	Thickness of TiO_2 CLs (nm)	Roughness (nm)
One	1	41	5.63
Two	1/2	50	4.62
Three	1/3	56	3.17
Four	1/4	65	3.36

Table 6. The mean values on V_{OC}, J_{SC}, FF and PCE of at least 25 PSCs under reverse scan. (Adapted from Ref. [223] by permission from Springer Nature, Journal of Materials Science: Materials in Electronics, Improved performance of perovskite solar cells by optimizing deposition parameters of TiO_2 compact layers, S. Li, et al., Copyright (2017)).

Deposition cycles of TiO_2 CLs	V_{OC} (V)	J_{SC} (mA/cm^2)	FF (%)	PCE (%)
One	0.98	18.67	69.91	12.84
Two	0.99	18.70	71.11	13.16
Three	1.01	19.13	72.64	14.04
Four	1.00	19.03	72.13	13.72

the J_{SC} of 8% higher than the fresh one. Aged sol produces thicker layers (15 nm) than the one fresh sol at similar spinning conditions due to its higher sol viscosity. However, the thickness of TiO_2 layers can be adapted by changing of the precursor concentration and spin coating speed. XPS analysis revealed that aged sol TiO_2 includes more defects than the fresh sol. Also, FTIR ATR spectroscopy indicted remained OH band in TiO_2 layers fabricated by aged sol even after calcination which proves the existence of residual crystalline water, leading to degradation of PSCs. Thus, the TiO_2 layer prepared by aged sol was replaced by a similar thickness of the fresh sol with the same performance. Chenxi Zhanget et al. [225] prepared TiO_2 CLs by various methods, a spin coating method by titaniumdiisopropoxide bis (acetylacetonate), CBD technique based on hydrolysis of $TiCl_4$, a sol-gel method by titanium isopropoxide and HCl, and screen-printing of titania paste, respectively. The surface morphologies of these CLs exhibited an important role in device efficiencies. The CL grown by the sol-gel method is rougher, thicker than the CBD

Table 7. Structures and photovoltaic parameters for PSCs with different fabrication methods.

Structure	J_{SC} (mA. cm^{-2})	V_{OC} (V)	FF	PCE (%)	References
FTO/TiO$_2$/TiO$_2$Mesoporous/CH$_3$NH$_3$PbI$_3$/ Spiro-OMTAD/Au	20.01	1	0.68	13.6	[192]
FTO/TiO$_2$/CH$_3$NH$_3$PbI$_3$/Spiro-OMTAD/Ag	18.57	0.96	0.49	8.7	[196]
ITO/TiO$_2$/CH$_3$NH$_3$PbI$_{3-X}$Cl$_x$/Spiro-OMTAD/Au	19.08	1	0.71	13.47	[198]
FTO/CdS/CH$_3$NH$_3$PbI$_3$/Spiro-OMTAD/Ag	8.51	0.52	0.51	2.27	[201]
FTO/TiO$_2$/TiO$_2$Mesoporous/CH$_3$NH$_3$PbI$_3$/ Spiro-OMTAD/Ag	20.81	1.03	0.70	15.03	[205]
FTO/SnO$_2$/CsMAFA/Spiro-OMTAD/Au	22	1.21	0.77	20.8	[209]
FTO/TiO$_2$/TiO$_2$Mesoporous/CH$_3$NH$_3$PbI$_3$/ Spiro-OMTAD/Au	21.97	1.09	0.63	15.07	[193]
FTO/TiO$_2$/TiO$_2$Mesoporous/CH$_3$NH$_3$PbI$_3$/ Spiro-OMTAD/Au	20.12	0.88	0.73	12.8	[210]
FTO/TiO$_2$/TiO$_2$Mesoporous/CH$_3$NH$_3$PbI$_3$/ Spiro-OMTAD/Ag	13.2	0.97	0.67	8.6	[212]
FTO/C$_{60}$/CH$_3$NH$_3$PbI$_3$/Spiro-OMTAD/Au	18.3	1.06	0.77	14.9	[215]
FTO/OA-freeTiO$_2$NCs/CsMAF/Spiro-OMTAD/Au	22.63	1.1	0.76	19.03	[216]
ITO/SnO$_2$/CH$_3$NH$_3$PbI$_3$/Spiro-OMTAD/Au	21.24	1.01	0.66	14.2	[219]
FTO/TiO$_2$/TiO$_2$/Mesoporous/CH$_3$NH$_3$PbI$_3$/ PMMA/Spiro-OMTAD/Au	22.1	0.93	0.59	13.6	[213]
FTO/TiO$_2$/TiO$_2$ Mesoporous/CH$_3$NH$_3$PbI$_3$/ Spiro-OMTAD/Ag	19.13	1.01	0.73	14.04	[223]
FTO/TiO$_2$/TiO$_2$Mesoporous/CH$_3$NH$_3$PbI$_3$/ Spiro-OMTAD/Au	21.1	0.91	0.54	10.32	[224]
FTO/TiO$_2$/TiO$_2$Mesoporous/theCH$_3$NH$_3$PbI$_{3-x}$Cl$_x$/ Spiro-OMTAD/AgAl	21.46	0.89	0.67	12.80	[225]

CL. The CL by the spin-coated produces amorphous TiOx films with porous structure and week coverage of FTO. The screen-printing CL displays a very rough structure with large cracks. The CL deposited by the CBD displayed rutile nanocrystalline TiO_2 film with superior morphological properties and effective electron collector along with highly efficient hole-blocking effect. Therefore, the CBD showed the best amount of PCE (12.80%) in comparison to the amount of PCE (10.48%, 9.05%, 8.92%) for Sol-gel, Spin-coating Screen-printing method, respectively. Table 7 summarizes structures and photovoltaic parameters in this section.

3. Conclusions

The most important issues regarding the development of PSCs are the improvement of efficiency, stability in order to industrialization. Different strategies have been presented for these issues involving using of various cations such as Cs^+, Li^+, Na^+, K^+ and Rb^+ in PSCs structures, some cations used instead of CH_3NH_3, $HC(CH_2)_2$, the replacing of lead with less toxic element such as Sn^{2+}, Cu^{2+}, Fe^{2+}, Ag^+, Ge^{2+}, Sr^{2+}, Bi^{3+}, Sb^{3+}, and also the utilization of different or mixed anions in perovskites structures. Moreover, simple methods for preparing cells such as screen-printing, spraying and ink-jet printing will help to industrialization. The improvement of stability by utilization of the encapsulation and suitable materials with high inherent stability will be useful to industrialization. Another strategy to improve efficiency is interfacial engineering via the material modification in every layer of PSCs (perovskite absorber, CL, mesoporous layer, and HTL) leading to appropriate energy level tuning between adjacent layers to decrease the energy loss, increase the electrical conductivity and passivate the trap states in the ETL and perovskite films. In this review, we investigated various materials as CLs and different strategies for improvement of their properties. The CL is an important layer in the PSCs to enhance application and efficiency. CLs should involve specific properties such as excellent charge carrier mobility, good transparency, and suitable level energy along with great stability. Also, low cost and low temperatures processes in combination with simple structures can increase their applications in flexible and roll-to-roll PSCs devices and achieve industrialization goal for PSCs. For high performance PSCs, a uniform, pinhole-free CL with superb electron transportability and a low recombination rate at the interface are very important. In order to enhance the PSCs performance, charge transport properties of the CL can be remarkably improved with replacing of some additives or dopants and using some thin wide bandgap metal oxide (e.g., MgO) as an interfacial layer. Also, interfacial modifications between the perovskite absorbers and charge transporting interlayers are very significant to enhance charge extraction and performance. CLs with the negligible density of oxygen vacancies with a larger band gap and expanded UV transparency, show a significant improvement in photo-stability and efficiency of converting light into electricity. It seems

that promising improvement in PSCs can be provided by research on CLs, especially in P-PSCs with simpler structures. The fabrication of CLs with high resistance against UV along with increased blocking ability and performance can be very much appreciated.

Declarations

Author contribution statement

All authors listed have significantly contributed to the development and the writing of this article.

Funding statement

Competing interest statement

The authors declare no conflict of interest.

Additional information

No additional information is available for this paper.

Acknowledgements

References

[1] A.E. Becquerel, The photovoltaic effect, Comptes Rendus 9 (1839) 145.

[2] L. Bu, Z. Liu, M. Zhang, W. Li, A. Zhu, F. Cai, Z. Zhao, Y. Zhou, Semi-transparent fully air processed perovskite solar cells, ACS Appl. Mater. Interfaces 7 (2015) 17776−17781.

[3] C.-Y. Chang, C.-Y. Chu, Y.-C. Huang, C.-W. Huang, S.-Y. Chang, C.-A. Chen, C.-Y. Chao, W.-F. Su, Tuning perovskite morphology by polymer additive for high efficiency solar cell, ACS Appl. Mater. Interfaces 7 (2015) 4955−4961.

[4] I. Hwang, I. Jeong, J. Lee, M.J. Ko, K. Yong, Enhancing stability of perovskite solar cells to moisture by the facile hydrophobic passivation, ACS Appl. Mater. Interfaces 7 (2015) 17330−17336.

[5] Y. Jin, G. Chumanov, Solution-processed planar perovskite solar cell without a hole transport layer, ACS Appl. Mater. Interfaces 7 (2015) 12015−12021.

[6] X. Hou, J. Zhou, S. Huang, W. Ou-Yang, L. Pan, X. Chen, Efficient quasi-mesoscopic perovskite solar cells using Li-doped hierarchical TiO2 as scaffold of scattered distribution, Chem. Eng. J. 330 (2017) 947−955.

[7] X. Hou, L. Pan, S. Huang, O.-Y. Wei, X. Chen, Enhanced efficiency and stability of perovskite solar cells using porous hierarchical TiO2 nanostructures of scattered distribution as scaffold, Electrochim. Acta 236 (2017) 351−358.

[8] M. Saliba, T. Matsui, K. Domanski, J.-Y. Seo, A. Ummadisingu, S.M. Zakeeruddin, J.-P. Correa-Baena, W.R. Tress, A. Abate, A. Hagfeldt, Incorporation of rubidium cations into perovskite solar cells improves photovoltaic performance, Science 354 (2016) 206−209.

[9] W. Zhou, J. Zhen, Q. Liu, Z. Fang, D. Li, P. Zhou, T. Chen, S. Yang, Successive surface engineering of TiO_2 compact layers via dual modification of fullerene derivatives affording hysteresis-suppressed high-performance perovskite solar cells, J. Mater. Chem. 5 (2017) 1724−1733.

[10] S.D. Stranks, G.E. Eperon, G. Grancini, C. Menelaou, M.J.P. Alcocer, T. Leijtens, L.M. Herz, A. Petrozza, H.J. Snaith, Electron-hole diffusion lengths exceeding 1 micrometer in an organometal trihalide perovskite absorber, Science 342 (2013) 341−344.

[11] Y. Da, Y. Xuan, Q. Li, Quantifying energy losses in planar perovskite solar cells, Sol. Energy Mater. Sol. Cell. 174 (2018) 206−213.

[12] L. Chen, F. Tang, Y. Wang, S. Gao, W. Cao, J. Cai, L. Chen, Facile preparation of organometallic perovskite films and high-efficiency solar cells using solid-state chemistry, Nano Res. 8 (2015) 263−270.

[13] B.C. O'Regan, J.R. Durrant, Kinetic and energetic paradigms for dye-sensitized solar cells: moving from the ideal to the real, Acc. Chem. Res. 42 (2009) 1799−1808.

[14] J. Nissfolk, K. Fredin, A. Hagfeldt, G. Boschloo, Recombination and transport processes in dye-sensitized solar cells investigated under working conditions, J. Phys. Chem. B 110 (2006) 17715−17718.

[15] D. Bi, L. Yang, G. Boschloo, A. Hagfeldt, E.M.J. Johansson, Effect of different hole transport materials on recombination in $CH_3NH_3PbI_3$ perovskite-sensitized mesoscopic solar cells, J. Phys. Chem. Lett. 4 (2013) 1532−1536.

[16] Y. Wu, X. Yang, H. Chen, K. Zhang, C. Qin, J. Liu, W. Peng, A. Islam, E. Bi, F. Ye, Highly compact TiO_2 layer for efficient hole-blocking in perovskite solar cells, APEX 7 (2014) 52301.

[17] B. O'regan, M. Grätzel, A low-cost, high-efficiency solar cell based on dye-sensitized colloidal TiO_2 films, Nature 353 (1991) 737.

[18] W. Li, J. Fan, J. Li, Y. Mai, L. Wang, Controllable grain morphology of perovskite absorber film by molecular self-assembly toward efficient solar cell exceeding 17%, J. Am. Chem. Soc. 137 (2015) 10399−10405.

[19] L. Kavan, N. Tétreault, T. Moehl, M. Grätzel, Electrochemical characterization of TiO_2 blocking layers for dye-sensitized solar cells, J. Phys. Chem. C 118 (2014) 16408−16418.

[20] X. Wang, Y. Fang, L. He, Q. Wang, T. Wu, Influence of compact TiO_2 layer on the photovoltaic characteristics of the organometal halide perovskite-based solar cells, Mater. Sci. Semicond. Process. 27 (2014) 569−576.

[21] D. Liu, T.L. Kelly, Perovskite solar cells with a planar heterojunction structure prepared using room-temperature solution processing techniques, Nat. Photon. 8 (2014) 133.

[22] Y. Rong, Z. Ku, A. Mei, T. Liu, M. Xu, S. Ko, X. Li, H. Han, Hole-conductor-free mesoscopic $TiO_2/CH_3NH_3PbI_3$ heterojunction solar cells based on anatase nanosheets and carbon counter electrodes, J. Phys. Chem. Lett. 5 (2014) 2160−2164.

[23] J.W. Jung, C. Chueh, A.K. Jen, A. Low-Temperature, Solution-Processable, Cu-Doped nickel oxide hole-transporting layer via the combustion method for high-performance thin-film perovskite solar cells, Adv. Mater. 27 (2015) 7874−7880.

[24] X. Chen, L.J. Tang, S. Yang, Y. Hou, H.G. Yang, A low-temperature processed flower-like TiO_2 array as an electron transport layer for high-performance perovskite solar cells, J. Mater. Chem. 4 (2016) 6521−6526.

[25] H. Zhou, Q. Chen, G. Li, S. Luo, T. Song, H.-S. Duan, Z. Hong, J. You, Y. Liu, Y. Yang, Interface engineering of highly efficient perovskite solar cells, Science 345 (2014) 542−546.

[26] H.-L. Yip, A.K.-Y. Jen, Recent advances in solution-processed interfacial materials for efficient and stable polymer solar cells, Energy Environ. Sci. 5 (2012) 5994−6011.

[27] M. Graetzel, R.A.J. Janssen, D.B. Mitzi, E.H. Sargent, Materials interface engineering for solution-processed photovoltaics, Nature 488 (2012) 304.

[28] C.-C. Chueh, C.-Z. Li, A.K.-Y. Jen, Recent progress and perspective in solution-processed Interfacial materials for efficient and stable polymer and organometal perovskite solar cells, Energy Environ. Sci. 8 (2015) 1160−1189.

[29] J. Shi, J. Liang, S. Peng, W. Xu, J. Pei, J. Chen, Synthesis, characterization and electrochemical properties of a compact titanium dioxide layer, Solid State Sci. 11 (2009) 433−438.

[30] J. Krüger, R. Plass, L. Cevey, M. Piccirelli, M. Grätzel, U. Bach, High efficiency solid-state photovoltaic device due to inhibition of interface charge recombination, Appl. Phys. Lett. 79 (2001) 2085−2087.

[31] L. Kavan, M. Grätzel, Highly efficient semiconducting TiO$_2$ photoelectrodes prepared by aerosol pyrolysis, Electrochim. Acta 40 (1995) 643−652.

[32] J.N. Hart, D. Menzies, Y.-B. Cheng, G.P. Simon, L. Spiccia, TiO$_2$ sol−gel blocking layers for dye-sensitized solar cells, Compt. Rendus Chem. 9 (2006) 622−626.

[33] P.J. Cameron, L.M. Peter, Characterization of titanium dioxide blocking layers in dye-sensitized nanocrystalline solar cells, J. Phys. Chem. B 107 (2003) 14394−14400.

[34] A. Hagfeldt, G. Boschloo, L. Sun, L. Kloo, H. Pettersson, Dye-sensitized solar cells, Chem. Rev. 110 (2010) 6595−6663.

[35] M. Yavari, M. Mazloum-Ardakani, S. Gholipour, N. Marinova, J.L. Delgado, S. Turren-Cruz, K. Domanski, N. Taghavinia, M. Saliba, M. Grätzel, Carbon nanoparticles in high-performance perovskite solar cells, Adv. Energy Mater. (2018).

[36] J.P.C. Baena, L. Steier, W. Tress, M. Saliba, S. Neutzner, T. Matsui, F. Giordano, T.J. Jacobsson, A.R.S. Kandada, S.M. Zakeeruddin, Highly efficient planar perovskite solar cells through band alignment engineering, Energy Environ. Sci. 8 (2015) 2928−2934.

[37] W. Li, W. Zhang, S. Van Reenen, R.J. Sutton, J. Fan, A.A. Haghighirad, M.B. Johnston, L. Wang, H.J. Snaith, Enhanced UV-light stability of planar heterojunction perovskite solar cells with caesium bromide interface modification, Energy Environ. Sci. 9 (2016) 490−498.

[38] M.J. Carnie, C. Charbonneau, M.L. Davies, J. Troughton, T.M. Watson, K. Wojciechowski, H. Snaith, D.A. Worsley, A one-step low temperature processing route for organolead halide perovskite solar cells, Chem. Commun. 49 (2013) 7893−7895.

[39] J.M. Ball, M.M. Lee, A. Hey, H.J. Snaith, Low-temperature processed meso-superstructured to thin-film perovskite solar cells, Energy Environ. Sci. 6 (2013) 1739−1743.

[40] J.T.-W. Wang, J.M. Ball, E.M. Barea, A. Abate, J.A. Alexander-Webber, J. Huang, M. Saliba, I. Mora-Sero, J. Bisquert, H.J. Snaith, Low-temperature processed electron collection layers of graphene/TiO$_2$ nanocomposites in thin film perovskite solar cells, Nano Lett. 14 (2013) 724−730.

[41] S. Dharani, H.K. Mulmudi, N. Yantara, P.T.T. Trang, N.G. Park, M. Graetzel, S. Mhaisalkar, N. Mathews, P.P. Boix, High efficiency electro-spun TiO$_2$ nanofiber based hybrid organic−inorganic perovskite solar cell, Nanoscale 6 (2014) 1675−1679.

[42] M. Dürr, A. Schmid, M. Obermaier, S. Rosselli, A. Yasuda, G. Nelles, Low-temperature fabrication of dye-sensitized solar cells by transfer of composite porous layers, Nat. Mater. 4 (2005) 607.

[43] G. Murugadoss, G. Mizuta, S. Tanaka, H. Nishino, T. Umeyama, H. Imahori, S. Ito, Double functions of porous TiO$_2$ electrodes on CH$_3$NH$_3$PbI$_3$ perovskite solar cells: enhancement of perovskite crystal transformation and prohibition of short circuiting, Apl. Mater. 2 (2014) 81511.

[44] L. Wang, W. Fu, Z. Gu, C. Fan, X. Yang, H. Li, H. Chen, Low temperature solution processed planar heterojunction perovskite solar cells with a CdSe nanocrystal as an electron transport/extraction layer, J. Mater. Chem. C 2 (2014) 9087−9090.

[45] R. Zhou, R. Stalder, D. Xie, W. Cao, Y. Zheng, Y. Yang, M. Plaisant, P.H. Holloway, K.S. Schanze, J.R. Reynolds, Enhancing the efficiency of solution-processed polymer: colloidal nanocrystal hybrid photovoltaic cells using ethanedithiol treatment, ACS Nano 7 (2013) 4846−4854.

[46] W.U. Huynh, J.J. Dittmer, A.P. Alivisatos, Hybrid nanorod-polymer solar cells, Science 295 (2002) 2425−2427.

[47] W.-F. Fu, Y. Shi, L. Wang, M.-M. Shi, H.-Y. Li, H.-Z. Chen, A green, low-cost, and highly effective strategy to enhance the performance of hybrid solar cells: post-deposition ligand exchange by acetic acid, Sol. Energy Mater. Sol. Cell. 117 (2013) 329−335.

[48] W. Fu, Y. Shi, W. Qiu, L. Wang, Y. Nan, M. Shi, H. Li, H. Chen, High efficiency hybrid solar cells using post-deposition ligand exchange by mono-thiols, Phys. Chem. Chem. Phys. 14 (2012) 12094−12098.

[49] Q. Dong, Y. Shi, K. Wang, Y. Li, S. Wang, H. Zhang, Y. Xing, Y. Du, X. Bai, T. Ma, Insight into perovskite solar cells based on SnO_2 compact electron-selective layer, J. Phys. Chem. C 119 (2015) 10212−10217.

[50] Q. Dong, M. Wang, Q. Zhang, F. Chen, S. Zhang, J. Bian, T. Ma, L. Wang, Y. Shi, Discontinuous SnO_2 derived blended-interfacial-layer in mesoscopic perovskite solar cells: minimizing electron transfer resistance and improving stability, Nano Energy 38 (2017) 358−367.

[51] J. Yang, B.D. Siempelkamp, E. Mosconi, F. De Angelis, T.L. Kelly, Origin of the thermal instability in $CH_3NH_3PbI_3$ thin films deposited on ZnO, Chem. Mater. 27 (2015) 4229−4236.

[52] J. Dong, Y. Zhao, J. Shi, H. Wei, J. Xiao, X. Xu, J. Luo, J. Xu, D. Li, Y. Luo, Impressive enhancement in the cell performance of ZnO nanorod-based perovskite solar cells with Al-doped ZnO interfacial modification, Chem. Commun. 50 (2014) 13381−13384.

[53] Y. Cheng, Q.-D. Yang, J. Xiao, Q. Xue, H.-W. Li, Z. Guan, H.-L. Yip, S.-W. Tsang, Decomposition of organometal halide perovskite films on zinc oxide nanoparticles, ACS Appl. Mater. Interfaces 7 (2015) 19986−19993.

[54] X. Zhao, H. Shen, Y. Zhang, X. Li, X. Zhao, M. Tai, J. Li, J. Li, X. Li, H. Lin, Aluminum-doped zinc oxide as highly stable electron collection layer for perovskite solar cells, ACS Appl. Mater. Interfaces 8 (2016) 7826−7833.

[55] H. Zhou, Y. Shi, K. Wang, Q. Dong, X. Bai, Y. Xing, Y. Du, T. Ma, Low-temperature processed and carbon-based $ZnO/CH_3NH_3PbI_3/C$ planar hetero-junction perovskite solar cells, J. Phys. Chem. C 119 (2015) 4600−4605.

[56] J. You, L. Meng, T.-B. Song, T.-F. Guo, Y.M. Yang, W.-H. Chang, Z. Hong, H. Chen, H. Zhou, Q. Chen, Improved air stability of perovskite solar cells via solution-processed metal oxide transport layers, Nat. Nanotechnol. 11 (2016) 75.

[57] D.-Y. Son, J.-H. Im, H.-S. Kim, N.-G. Park, 11% efficient perovskite solar cell based on ZnO nanorods: an effective charge collection system, J. Phys. Chem. C 118 (2014) 16567−16573.

[58] K. Mahmood, B.S. Swain, A. Amassian, 16.1% efficient hysteresis-free mes-ostructured perovskite solar cells based on synergistically improved ZnO nanorod arrays, Adv. Energy Mater. 5 (2015).

[59] D. Liu, J. Yang, T.L. Kelly, Compact layer free perovskite solar cells with 13.5% efficiency, J. Am. Chem. Soc. 136 (2014) 17116−17122.

[60] Q. Hu, J. Wu, C. Jiang, T. Liu, X. Que, R. Zhu, Q. Gong, Engineering of electron-selective contact for perovskite solar cells with efficiency exceeding 15%, ACS Nano 8 (2014) 10161−10167.

[61] J. Cao, B. Wu, R. Chen, Y. Wu, Y. Hui, B. Mao, N. Zheng, Efficient, hysteresis-free, and stable perovskite solar cells with ZnO as electron-transport layer: effect of surface passivation, Adv. Mater. (2018).

[62] G.S. Han, H.S. Chung, B.J. Kim, D.H. Kim, J.W. Lee, B.S. Swain, K. Mahmood, J.S. Yoo, N.-G. Park, J.H. Lee, Retarding charge recombination in perovskite solar cells using ultrathin MgO-coated TiO_2 nanoparticulate films, J. Mater. Chem. 3 (2015) 9160−9164.

[63] X. Guo, H. Dong, W. Li, N. Li, L. Wang, Multifunctional MgO layer in perovskite solar cells, ChemPhysChem 16 (2015) 1727−1732.

[64] Y. Gao, Z. Dai, J. Zhang, X. Ma, N. Tang, J. Wu, Trinuclear and tetranuclear magnesium alkoxide clusters as highly active initiators for ring-opening polymerization of L-lactide, Inorg. Chem. 53 (2013) 716−726.

[65] W. Li, Q. Jiang, J. Yang, Y. Luo, X. Li, Y. Hou, S. Zhou, Improvement of photovoltaic performance of perovskite solar cells with a ZnO/Zn_2SnO_4 composite compact layer, Sol. Energy Mater. Sol. Cell. 159 (2017) 143−150.

[66] L. Loh, J. Briscoe, S. Dunn, Chemical protection of ZnO nanorods at ultralow pH to form a hierarchical $BiFeO_3$/ZnO core−shell structure, ACS Appl. Mater. Interfaces 7 (2015) 152−157.

[67] F. Di Giacomo, V. Zardetto, A. D'Epifanio, S. Pescetelli, F. Matteocci, S. Razza, A. Di Carlo, S. Licoccia, W.M.M. Kessels, M. Creatore, Flexible perovskite photovoltaic modules and solar cells based on atomic layer deposited compact layers and UV-irradiated TiO_2 scaffolds on plastic substrates, Adv. Energy Mater. (2015) 5.

[68] A.H. Ip, S.M. Thon, S. Hoogland, O. Voznyy, D. Zhitomirsky, R. Debnath, L. Levina, L.R. Rollny, G.H. Carey, A. Fischer, Hybrid passivated colloidal quantum dot solids, Nat. Nanotechnol. 7 (2012) 577.

[69] J. Gao, C.L. Perkins, J.M. Luther, M.C. Hanna, H.-Y. Chen, O.E. Semonin, A.J. Nozik, R.J. Ellingson, M.C. Beard, n-Type transition metal oxide as a hole extraction layer in PbS quantum dot solar cells, Nano Lett. 11 (2011) 3263−3266.

[70] Y. Tu, J. Wu, M. Zheng, J. Huo, P. Zhou, Z. Lan, J. Lin, M. Huang, TiO_2 quantum dots as superb compact block layers for high-performance $CH_3NH_3PbI_3$ perovskite solar cells with an efficiency of 16.97%, Nanoscale 7 (2015) 20539−20546.

[71] K. Wang, C. Liu, P. Du, J. Zheng, X. Gong, Bulk heterojunction perovskite hybrid solar cells with large fill factor, Energy Environ. Sci. 8 (2015) 1245−1255.

[72] W. Ke, G. Fang, Q. Liu, L. Xiong, P. Qin, H. Tao, J. Wang, H. Lei, B. Li, J. Wan, Low-temperature solution-processed tin oxide as an alternative electron transporting layer for efficient perovskite solar cells, J. Am. Chem. Soc. 137 (2015) 6730−6733.

[73] B.J. Kim, D.H. Kim, Y.-Y. Lee, H.-W. Shin, G.S. Han, J.S. Hong, K. Mahmood, T.K. Ahn, Y.-C. Joo, K.S. Hong, Highly efficient and bending durable perovskite solar cells: toward a wearable power source, Energy Environ. Sci. 8 (2015) 916−921.

[74] F. Gao, H. Dai, H. Pan, Y. Chen, J. Wang, Z. Chen, Performance enhancement of perovskite solar cells by employing TiO_2 nanorod arrays decorated with $CuInS_2$ quantum dots, J. Colloid Interface Sci. 513 (2018) 693−699.

[75] I. Konovalov, Material requirements for CIS solar cells, Thin Solid Films 451 (2004) 413−419.

[76] T. Leijtens, B. Lauber, G.E. Eperon, S.D. Stranks, H.J. Snaith, The importance of perovskite pore filling in organometal mixed halide sensitized TiO_2-based solar cells, J. Phys. Chem. Lett. 5 (2014) 1096−1102.

[77] H. Li, W. Shi, W. Huang, E.-P. Yao, J. Han, Z. Chen, S. Liu, Y. Shen, M. Wang, Y. Yang, Carbon quantum dots/TiO_x electron transport layer boosts efficiency of planar heterojunction perovskite solar cells to 19%, Nano Lett. 17 (2017) 2328−2335.

[78] D. Tang, J. Liu, X. Wu, R. Liu, X. Han, Y. Han, H. Huang, Y. Liu, Z. Kang, Carbon quantum dot/NiFe layered double-hydroxide composite as a highly efficient electrocatalyst for water oxidation, ACS Appl. Mater. Interfaces 6 (2014) 7918−7925.

[79] G. Xing, B. Wu, S. Chen, J. Chua, N. Yantara, S. Mhaisalkar, N. Mathews, T.C. Sum, Interfacial electron transfer barrier at compact TiO_2/$CH_3NH_3PbI_3$ heterojunction, Small 11 (2015) 3606−3613.

[80] J. Jeng, Y. Chiang, M. Lee, S. Peng, T. Guo, P. Chen, T. Wen, $CH_3NH_3PbI_3$ perovskite/fullerene planar-heterojunction hybrid solar cells, Adv. Mater. 25 (2013) 3727−3732.

[81] P. Docampo, J.M. Ball, M. Darwich, G.E. Eperon, H.J. Snaith, Efficient organometal trihalide perovskite planar-heterojunction solar cells on flexible polymer substrates, Nat. Commun. 4 (2013) 2761.

[82] C. Bi, Q. Wang, Y. Shao, Y. Yuan, Z. Xiao, J. Huang, Non-wetting surface-driven high-aspect-ratio crystalline grain growth for efficient hybrid perovskite solar cells, Nat. Commun. 6 (2015) 7747.

[83] Y. Shao, Y. Yuan, J. Huang, Correlation of energy disorder and open-circuit voltage in hybrid perovskite solar cells, Nat. Energy 1 (2016) 15001.

[84] C. Wang, J. Zhang, G. Long, N. Aratani, H. Yamada, Y. Zhao, Q. Zhang, Synthesis, structure, and air-stable N-type field-effect transistor behaviors of functionalized octaazanonacene-8, 19-dione, Angew. Chem. Int. Ed. 54 (2015) 6292−6296.

[85] M. Saliba, S. Orlandi, T. Matsui, S. Aghazada, M. Cavazzini, J.-P. Correa-Baena, P. Gao, R. Scopelliti, E. Mosconi, K.-H. Dahmen, A molecularly engineered hole-transporting material for efficient perovskite solar cells, Nat. Energy 1 (2016) 15017.

[86] N.K. Noel, A. Abate, S.D. Stranks, E.S. Parrott, V.M. Burlakov, A. Goriely, H.J. Snaith, Enhanced photoluminescence and solar cell performance via Lewis base passivation of organic−inorganic lead halide perovskites, ACS Nano 8 (2014) 9815−9821.

[87] N. Wang, K. Zhao, T. Ding, W. Liu, A.S. Ahmed, Z. Wang, M. Tian, X.W. Sun, Q. Zhang, Improving interfacial charge recombination in planar heterojunction perovskite photovoltaics with small molecule as electron transport layer, Adv. Energy Mater. 7 (2017).

[88] J. Jeng, K. Chen, T. Chiang, P. Lin, T. Tsai, Y. Chang, T. Guo, P. Chen, T. Wen, Y. Hsu, Nickel oxide electrode interlayer in $CH_3NH_3PbI_3$ perovskite/PCBM planar-heterojunction hybrid solar cells, Adv. Mater. 26 (2014) 4107−4113.

[89] J. Xu, A. Buin, A.H. Ip, W. Li, O. Voznyy, R. Comin, M. Yuan, S. Jeon, Z. Ning, J.J. McDowell, Perovskite−fullerene hybrid materials suppress hysteresis in planar diodes, Nat. Commun. 6 (2015) 7081.

[90] M. Shahiduzzaman, M. Karakawa, K. Yamamoto, T. Kusumi, K. Yonezawa, T. Kuwabara, K. Takahashi, T. Taima, Interface engineering of compact-TiO_x in planar perovskite solar cells using low-temperature processable high-mobility fullerene derivative, Sol. Energy Mater. Sol. Cell. 178 (2018) 1−7.

[91] A. Kogo, Y. Numata, M. Ikegami, T. Miyasaka, Nb_2O_5 blocking layer for high open-circuit voltage perovskite solar cells, Chem. Lett. 44 (2015) 829−830.

[92] H. Tan, A. Jain, O. Voznyy, X. Lan, F.P.G. de Arquer, J.Z. Fan, R. Quintero-Bermudez, M. Yuan, B. Zhang, Y. Zhao, Efficient and stable solution-processed planar perovskite solar cells via contact passivation, Science 355 (2017) 722−726.

[93] J. Wang, J. Polleux, J. Lim, B. Dunn, Pseudocapacitive contributions to electrochemical energy storage in TiO_2 (anatase) nanoparticles, J. Phys. Chem. C 111 (2007) 14925−14931.

[94] M. Niederberger, M.H. Bartl, G.D. Stucky, Benzyl alcohol and titanium tetrachloride a versatile reaction system for the nonaqueous and low-temperature preparation of crystalline and luminescent titania nanoparticles, Chem. Mater. 14 (2002) 4364−4370.

[95] E. Mosconi, E. Ronca, F. De Angelis, First-principles investigation of the TiO_2/organohalide perovskites interface: the role of interfacial chlorine, J. Phys. Chem. Lett. 5 (2014) 2619−2625.

[96] M.M. Byranvand, T. Kim, S. Song, G. Kang, S.U. Ryu, T. Park, p-Type CuI islands on TiO_2 electron transport layer for a highly efficient planar-perovskite solar cell with negligible hysteresis, Adv. Energy Mater. 8 (2018).

[97] J.A. Christians, R.C.M. Fung, P. V Kamat, An inorganic hole conductor for organo-lead halide perovskite solar cells. Improved hole conductivity with copper iodide, J. Am. Chem. Soc. 136 (2013) 758−764.

[98] A. Paulke, S.D. Stranks, J. Kniepert, J. Kurpiers, C.M. Wolff, N. Schön, H.J. Snaith, T.J.K. Brenner, D. Neher, Charge Carrier recombination dynamics in perovskite and polymer solar cells, Appl. Phys. Lett. 108 (2016) 113505.

[99] M. Li, Z.-K. Wang, T. Kang, Y. Yang, X. Gao, C.-S. Hsu, Y. Li, L.-S. Liao, Graphdiyne-modified cross-linkable fullerene as an efficient electron-transporting layer in organometal halide perovskite solar cells, Nano Energy 43 (2018) 47−54.

[100] C. Tao, J. Van Der Velden, L. Cabau, N.F. Montcada, S. Neutzner, S. Kandada, A. Ram, S. Marras, L. Brambilla, M. Tommasini, Fully solution-processed n−i−p-Like perovskite solar cells with planar junction: how the charge extracting layer determines the open-circuit voltage, Adv. Mater. 29 (2017).

[101] M. Li, Y.-H. Chao, T. Kang, Z.-K. Wang, Y.-G. Yang, S.-L. Feng, Y. Hu, X.-Y. Gao, L.-S. Liao, C.-S. Hsu, Enhanced crystallization and stability of perovskites by a cross-linkable fullerene for high-performance solar cells, J. Mater. Chem. 4 (2016) 15088−15094.

[102] Y.-J. Cheng, C.-H. Hsieh, Y. He, C.-S. Hsu, Y. Li, Combination of indene-C60 bis-adduct and cross-linked fullerene interlayer leading to highly efficient inverted polymer solar cells, J. Am. Chem. Soc. 132 (2010) 17381−17383.

[103] Y. Zhou, K. Zhu, Perovskite solar cells shine in the "Valley of the Sun, ACS Energy Lett. 1 (2016) 64−67.

[104] T. Leijtens, G.E. Eperon, S. Pathak, A. Abate, M.M. Lee, H.J. Snaith, Overcoming ultraviolet light instability of sensitized TiO_2 with meso-superstructured organometal tri-halide perovskite solar cells, Nat. Commun. 4 (2013) 2885.

[105] N. Chander, A.F. Khan, P.S. Chandrasekhar, E. Thouti, S.K. Swami, V. Dutta, V.K. Komarala, Reduced ultraviolet light induced degradation and enhanced light harvesting using YVO_4: Eu^{3+} down-shifting nano-phosphor layer in organometal halide perovskite solar cells, Appl. Phys. Lett. 105 (2014) 33904.

[106] B. Roose, J.-P.C. Baena, K.C. Gödel, M. Graetzel, A. Hagfeldt, U. Steiner, A. Abate, Mesoporous SnO_2 electron selective contact enables UV-stable perovskite solar cells, Nano Energy 30 (2016) 517−522.

[107] S. Ito, S. Tanaka, K. Manabe, H. Nishino, Effects of surface blocking layer of Sb2S3 on nanocrystalline TiO_2 for $CH_3NH_3PbI_3$ perovskite solar cells, J. Phys. Chem. C 118 (2014) 16995−17000.

[108] S.S. Shin, E.J. Yeom, W.S. Yang, S. Hur, M.G. Kim, J. Im, J. Seo, J.H. Noh, S. Il Seok, Colloidally prepared La-doped $BaSnO_3$ electrodes for efficient, photostable perovskite solar cells, Science 356 (2017) 167−171.

[109] Q. Luo, H. Chen, Y. Lin, H. Du, Q. Hou, F. Hao, N. Wang, Z. Guo, J. Huang, Discrete iron (III) oxide nanoislands for efficient and photostable perovskite solar cells, Adv. Funct. Mater. 27 (2017).

[110] K. Sivula, F. Le Formal, M. Grätzel, Solar water splitting: progress using hematite (α-Fe_2O_3) photoelectrodes, ChemSusChem 4 (2011) 432−449.

[111] M. Grätzel, Photoelectrochemical cells, Nature 414 (2001) 338.

[112] M.J. Katz, S.C. Riha, N.C. Jeong, A.B.F. Martinson, O.K. Farha, J.T. Hupp, Toward solar fuels: water splitting with sunlight and "rust", Coord. Chem. Rev. 256 (2012) 2521−2529.

[113] B. Wu, K. Fu, N. Yantara, G. Xing, S. Sun, T.C. Sum, N. Mathews, Charge accumulation and hysteresis in perovskite-based solar cells: an electro-optical analysis, Adv. Energy Mater. 5 (2015).

[114] Q. Luo, H. Ma, Y. Zhang, X. Yin, Z. Yao, N. Wang, J. Li, S. Fan, K. Jiang, H. Lin, Cross-stacked superaligned carbon nanotube electrodes for efficient hole conductor-free perovskite solar cells, J. Mater. Chem. 4 (2016) 5569−5577.

[115] H.-S. Kim, I.-H. Jang, N. Ahn, M. Choi, A. Guerrero, J. Bisquert, N.-G. Park, Control of I−V hysteresis in $CH_3NH_3PbI_3$ perovskite solar cell, J. Phys. Chem. Lett. 6 (2015) 4633−4639.

[116] S.S. Shin, W.S. Yang, J.H. Noh, J.H. Suk, N.J. Jeon, J.H. Park, J.S. Kim, W.M. Seong, S. Il Seok, High-performance flexible perovskite solar cells exploiting Zn_2 SnO_4 prepared in solution below 100 °C, Nat. Commun. 6 (2015) 7410.

[117] K. Wang, Y. Shi, B. Li, L. Zhao, W. Wang, X. Wang, X. Bai, S. Wang, C. Hao, T. Ma, Amorphous inorganic electron-selective layers for efficient perovskite solar cells: feasible strategy towards room-temperature fabrication, Adv. Mater. 28 (2016) 1891−1897.

[118] I. Hwang, K. Yong, Novel CdS hole-blocking layer for photostable perovskite solar cells, ACS Appl. Mater. Interfaces 8 (2016) 4226−4232.

[119] J.H. Heo, H.J. Han, D. Kim, T.K. Ahn, S.H. Im, Hysteresis-less inverted $CH_3NH_3PbI_3$ planar perovskite hybrid solar cells with 18.1% power conversion efficiency, Energy Environ. Sci. 8 (2015) 1602−1608.

[120] T. Chen, C. Lin, S. Li, Y. Tsai, C. Wen, W.J. Lin, F. Hsiao, Y. Chiu, K. Tsukagoshi, M. Osada, Self-Assembly atomic stacking transport layer of 2D layered titania for perovskite solar cells with extended UV stability, Adv. Energy Mater. 8 (2018).

[121] M. Osada, Y. Ebina, H. Funakubo, S. Yokoyama, T. Kiguchi, K. Takada, T. Sasaki, High-κ dielectric nanofilms fabricated from titania nanosheets, Adv. Mater. 18 (2006) 1023−1027.

[122] M. Osada, T. Sasaki, Two-dimensional dielectric nanosheets: novel nanoelectronics from nanocrystal building blocks, Adv. Mater. 24 (2012) 210−228.

[123] X. Liu, T. Bu, J. Li, J. He, T. Li, J. Zhang, W. Li, Z. Ku, Y. Peng, F. Huang, Stacking n-type layers: effective route towards stable, efficient and hysteresis-free planar perovskite solar cells, Nano Energy 44 (2018) 34−42.

[124] X. Xu, H. Zhang, J. Shi, J. Dong, Y. Luo, D. Li, Q. Meng, Highly efficient planar perovskite solar cells with a TiO_2/ZnO electron transport bilayer, J. Mater. Chem. 3 (2015) 19288−19293.

[125] A. Kogo, M. Ikegami, T. Miyasaka, A SnO x−brookite TiO$_2$ bilayer electron collector for hysteresis-less high efficiency plastic perovskite solar cells fabricated at low process temperature, Chem. Commun. 52 (2016) 8119−8122.

[126] M. Saliba, T. Matsui, J.-Y. Seo, K. Domanski, J.-P. Correa-Baena, M.K. Nazeeruddin, S.M. Zakeeruddin, W. Tress, A. Abate, A. Hagfeldt, Cesium-containing triple cation perovskite solar cells: improved stability, reproducibility and high efficiency, Energy Environ. Sci. 9 (2016) 1989−1997.

[127] W. Chu, J. Yang, Q. Jiang, X. Li, J. Xin, Enhancement of Photovoltaic Performance of flexible Perovskite solar cells by means of Ionic liquid interface modification in a low temperature all solution process, Appl. Surf. Sci. (2018).

[128] M.A. Mahmud, N.K. Elumalai, M.B. Upama, D. Wang, V.R. Gonçales, M. Wright, J.J. Gooding, F. Haque, C. Xu, A. Uddin, Cesium compounds as interface modifiers for stable and efficient perovskite solar cells, Sol. Energy Mater. Sol. Cell. 174 (2018) 172−186.

[129] F. Huang, Y. Dkhissi, W. Huang, M. Xiao, I. Benesperi, S. Rubanov, Y. Zhu, X. Lin, L. Jiang, Y. Zhou, Gas-assisted preparation of lead iodide perovskite films consisting of a monolayer of single crystalline grains for high efficiency planar solar cells, Nano Energy 10 (2014) 10−18.

[130] J. Kim, G. Kim, T.K. Kim, S. Kwon, H. Back, J. Lee, S.H. Lee, H. Kang, K. Lee, Efficient planar-heterojunction perovskite solar cells achieved via interfacial modification of a sol−gel ZnO electron collection layer, J. Mater. Chem. 2 (2014) 17291−17296.

[131] T. Hu, S. Xiao, H. Yang, L. Chen, Y. Chen, Cerium oxide as an efficient electron extraction layer for p−i−n structured perovskite solar cells, Chem. Commun. 54 (2018) 471−474.

[132] H. Il Kim, M. Kim, K. Choi, C. Lim, Y. Kim, S. Kwon, T. Park, Improving the performance and stability of inverted planar flexible perovskite solar cells employing a novel NDI-based polymer as the electron transport layer, Adv. Energy Mater. (2018).

[133] Y.H. Choi, H. Bin Kim, I.S. Yang, S. Do Sung, Y.S. Choi, J. Kim, W.I. Lee, Silicotungstate, a potential electron transporting layer for low-temperature perovskite solar cells, ACS Appl. Mater. Interfaces 9 (2017) 25257−25264.

[134] J. Song, S.P. Li, Y.L. Zhao, J. Yuan, Y. Zhu, Y. Fang, L. Zhu, X.Q. Gu, Y.H. Qiang, Performance enhancement of perovskite solar cells by doping TiO$_2$ blocking layer with group VB elements, J. Alloy. Comp. 694 (2017) 1232−1238.

[135] H. Zhang, J. Shi, X. Xu, L. Zhu, Y. Luo, D. Li, Q. Meng, Mg-doped TiO_2 boosts the efficiency of planar perovskite solar cells to exceed 19%, J. Mater. Chem. 4 (2016) 15383−15389.

[136] X. Yin, Y. Guo, Z. Xue, P. Xu, M. He, B. Liu, Performance enhancement of perovskite-sensitized mesoscopic solar cells using Nb-doped TiO_2 compact layer, Nano Res. 8 (2015) 1997−2003.

[137] W. Wang, H. Zheng, Y. Liu, J. Sun, L. Gao, Enhanced perovskite solar cells with cesium-doped TiO_2 compact layer, J. Nanosci. Nanotechnol. 16 (2016) 12768−12772.

[138] K. Manseki, T. Ikeya, A. Tamura, T. Ban, T. Sugiura, T. Yoshida, Mg-doped TiO_2 nanorods improving open-circuit voltages of ammonium lead halide perovskite solar cells, RSC Adv. 4 (2014) 9652−9655.

[139] B.-X. Chen, H.-S. Rao, W.-G. Li, Y.-F. Xu, H.-Y. Chen, D.-B. Kuang, C.-Y. Su, Achieving high-performance planar perovskite solar cell with Nb-doped TiO_2 compact layer by enhanced electron injection and efficient charge extraction, J. Mater. Chem. 4 (2016) 5647−5653.

[140] P. Qin, A.L. Domanski, A.K. Chandiran, R. Berger, H.-J. Butt, M.I. Dar, T. Moehl, N. Tetreault, P. Gao, S. Ahmad, Yttrium-substituted nanocrystalline TiO_2 photoanodes for perovskite based heterojunction solar cells, Nanoscale 6 (2014) 1508−1514.

[141] H. Li, B. Zheng, Y. Xue, S. Liu, C. Gao, X. Liu, Spray deposited lanthanum doped TiO_2 compact layers as electron selective contact for perovskite solar cells, Sol. Energy Mater. Sol. Cell. 168 (2017) 85−90.

[142] Y. Zhang, H. Zhang, Y. Xu, Y. Wang, Significant effect of lanthanide doping on the texture and properties of nanocrystalline mesoporous TiO_2, J. Solid State Chem. 177 (2004) 3490−3498.

[143] A.M. Ruiz, A. Cornet, J.R. Morante, Performances of La−TiO_2 nanoparticles as gas sensing material, Sensor. Actuator. B Chem. 111 (2005) 7−12.

[144] Y. Huo, J. Zhu, J. Li, G. Li, H. Li, An active La/TiO_2 photocatalyst prepared by ultrasonication-assisted sol−gel method followed by treatment under supercritical conditions, J. Mol. Catal. Chem. 278 (2007) 237−243.

[145] J. Wang, M. Qin, H. Tao, W. Ke, Z. Chen, J. Wan, P. Qin, L. Xiong, H. Lei, H. Yu, Performance enhancement of perovskite solar cells with Mg-doped TiO_2 compact film as the hole-blocking layer, Appl. Phys. Lett. 106 (2015) 121104.

[146] Y. Xiang, Z. Ma, J. Zhuang, H. Lu, C. Jia, J. Luo, H. Li, X. Cheng, Enhanced performance for planar perovskite solar cells with samarium-doped TiO_2 compact electron transport layers, J. Phys. Chem. C 121 (2017) 20150−20157.

[147] X. Ren, D. Yang, Z. Yang, J. Feng, X. Zhu, J. Niu, Y. Liu, W. Zhao, S.F. Liu, Solution-processed Nb: SnO_2 electron transport layer for efficient planar perovskite solar cells, ACS Appl. Mater. Interfaces 9 (2017) 2421−2429.

[148] R. Ranjan, A. Prakash, A. Singh, A. Singh, A. Garg, R.K. Gupta, Effect of tantalum doping in a TiO_2 compact layer on the performance of planar spiro-OMeTAD free perovskite solar cells, J. Mater. Chem. 6 (2018) 1037−1047.

[149] M. Yang, R. Guo, K. Kadel, Y. Liu, K. O'Shea, R. Bone, X. Wang, J. He, W. Li, Improved charge transport of Nb-doped TiO_2 nanorods in methylammonium lead iodide bromide perovskite solar cells, J. Mater. Chem. 2 (2014) 19616−19622.

[150] J. Saito, T. Oku, A. Suzuki, T. Akiyama, Fabrication and characterization of perovskite-type solar cells with Nb-doped TiO_2 layers, in: AIP Conference Proceedings, AIP Publishing, 2016, p. 20027.

[151] B. Roose, K.C. Gödel, S. Pathak, A. Sadhanala, J.P.C. Baena, B.D. Wilts, H.J. Snaith, U. Wiesner, M. Grätzel, U. Steiner, Enhanced efficiency and stability of perovskite solar cells through Nd-doping of mesostructured TiO_2, Adv. Energy Mater. 6 (2016).

[152] S.K. Pathak, A. Abate, P. Ruckdeschel, B. Roose, K.C. Gödel, Y. Vaynzof, A. Santhala, S. Watanabe, D.J. Hollman, N. Noel, Performance and stability enhancement of dye-sensitized and perovskite solar cells by Al doping of TiO_2, Adv. Funct. Mater. 24 (2014) 6046−6055.

[153] H. Nagaoka, F. Ma, D.W. deQuilettes, S.M. Vorpahl, M.S. Glaz, A.E. Colbert, M.E. Ziffer, D.S. Ginger, Zr incorporation into TiO_2 electrodes reduces hysteresis and improves performance in hybrid perovskite solar cells while increasing Carrier lifetimes, J. Phys. Chem. Lett. 6 (2015) 669−675.

[154] J. Hu, R. Gottesman, L. Gouda, A. Kama, M. Priel, S. Tirosh, J. Bisquert, A. Zaban, Photovoltage behavior in perovskite solar cells under light-soaking showing photoinduced interfacial changes, ACS Energy Lett. 2 (2017) 950−956.

[155] F. Giordano, A. Abate, J.P.C. Baena, M. Saliba, T. Matsui, S.H. Im, S.M. Zakeeruddin, M.K. Nazeeruddin, A. Hagfeldt, M. Graetzel, Enhanced

electronic properties in mesoporous TiO$_2$ via lithium doping for high-efficiency perovskite solar cells, Nat. Commun. 7 (2016) 10379.

[156] A. Baktash, O. Amiri, A. Sasani, Improve efficiency of perovskite solar cells by using magnesium doped ZnO and TiO$_2$ compact layers, Superlattice. Microst. 93 (2016) 128−137.

[157] C. Liang, P. Li, Y. Zhang, H. Gu, Q. Cai, X. Liu, J. Wang, H. Wen, G. Shao, Mild solution-processed metal-doped TiO$_2$ compact layers for hysteresis-less and performance-enhanced perovskite solar cells, J. Power Sources 372 (2017) 235−244.

[158] Q. Zhu, X. Bao, J. Yu, D. Zhu, M. Qiu, R. Yang, L. Dong, Compact layer free perovskite solar cells with a high-mobility hole-transporting layer, ACS Appl. Mater. Interfaces 8 (2016) 2652−2657.

[159] V. D'Innocenzo, G. Grancini, M.J.P. Alcocer, A.R.S. Kandada, S.D. Stranks, M.M. Lee, G. Lanzani, H.J. Snaith, A. Petrozza, Excitons versus free charges in organo-lead tri-halide perovskites, Nat. Commun. 5 (2014) 3586.

[160] L. Zheng, Y.-H. Chung, Y. Ma, L. Zhang, L. Xiao, Z. Chen, S. Wang, B. Qu, Q. Gong, A hydrophobic hole transporting oligothiophene for planar perovskite solar cells with improved stability, Chem. Commun. 50 (2014) 11196−11199.

[161] D.H. Cao, C.C. Stoumpos, C.D. Malliakas, M.J. Katz, O.K. Farha, J.T. Hupp, M.G. Kanatzidis, Remnant PbI$_2$, an unforeseen necessity in high-efficiency hybrid perovskite-based solar cells, Apl. Mater. 2 (2014) 91101.

[162] M.H. Kumar, N. Yantara, S. Dharani, M. Graetzel, S. Mhaisalkar, P.P. Boix, N. Mathews, Flexible, low-temperature, solution processed ZnO-based perovskite solid state solar cells, Chem. Commun. 49 (2013) 11089−11091.

[163] A. Kulkarni, A.K. Jena, H.-W. Chen, Y. Sanehira, M. Ikegami, T. Miyasaka, Revealing and reducing the possible recombination loss within TiO$_2$ compact layer by incorporating MgO layer in perovskite solar cells, Sol. Energy 136 (2016) 379−384.

[164] N. Yantara, D. Sabba, F. Yanan, J.M. Kadro, T. Moehl, P.P. Boix, S. Mhaisalkar, M. Grätzel, C. Grätzel, Loading of mesoporous titania films by CH$_3$NH$_3$PbI$_3$ perovskite, single step vs. sequential deposition, Chem. Commun. 51 (2015) 4603−4606.

[165] C. Wehrenfennig, C.M. Palumbiny, H.J. Snaith, M.B. Johnston, L. Schmidt-Mende, L.M. Herz, Fast charge-Carrier trapping in TiO$_2$ nanotubes, J. Phys. Chem. C 119 (2015) 9159−9168.

[166] X. Wang, Z. Feng, J. Shi, G. Jia, S. Shen, J. Zhou, C. Li, Trap states and Carrier dynamics of TiO_2 studied by photoluminescence spectroscopy under weak excitation condition, Phys. Chem. Chem. Phys. 12 (2010) 7083−7090.

[167] L. Bertoluzzi, I. Herraiz-Cardona, R. Gottesman, A. Zaban, J. Bisquert, Relaxation of electron carriers in the density of states of nanocrystalline TiO_2, J. Phys. Chem. Lett. 5 (2014) 689−694.

[168] R. Sandoval-Torrientes, J. Pascual, I. García-Benito, S. Collavini, I. Kosta, R. Tena-Zaera, N. Martín, J.L. Delgado, Modified fullerenes for efficient electron transport layer-free perovskite/fullerene blend-based solar cells, ChemSusChem 10 (2017) 2023−2029.

[169] L. Huang, Z. Hu, J. Xu, X. Sun, Y. Du, J. Ni, H. Cai, J. Li, J. Zhang, Efficient planar perovskite solar cells without a high temperature processed titanium dioxide electron transport layer, Sol. Energy Mater. Sol. Cell. 149 (2016) 1−8.

[170] H. Yu, J.W. Lee, J. Yun, K. Lee, J. Ryu, J. Lee, D. Hwang, S.K. Kim, J. Jang, Outstanding performance of hole-blocking layer-free perovskite solar cell using hierarchically porous fluorine-doped tin oxide substrate, Adv. Energy Mater. 7 (2017).

[171] G. Cheng, W.-Y. Tong, K.-H. Low, C.-M. Che, Thermal-annealing-free inverted polymer solar cells using ZnO/Cs_2CO_3 bilayer as electron-selective layer, Sol. Energy Mater. Sol. Cell. 103 (2012) 164−170.

[172] H.-H. Liao, L.-M. Chen, Z. Xu, G. Li, Y. Yang, Highly efficient inverted polymer solar cell by low temperature annealing of Cs_2CO_3 interlayer, Appl. Phys. Lett. 92 (2008) 156.

[173] H. Yu, J. Ryu, J.W. Lee, J. Roh, K. Lee, J. Yun, J. Lee, Y.K. Kim, D. Hwang, J. Kang, Large grain-based hole-blocking layer-free planar-type perovskite solar cell with best efficiency of 18.20%, ACS Appl. Mater. Interfaces 9 (2017) 8113−8120.

[174] H. Do Kim, H. Ohkita, H. Benten, S. Ito, Photovoltaic performance of perovskite solar cells with different grain sizes, Adv. Mater. 28 (2016) 917−922.

[175] L. Zuo, Z. Gu, T. Ye, W. Fu, G. Wu, H. Li, H. Chen, Enhanced photovoltaic performance of $CH_3NH_3PbI_3$ perovskite solar cells through interfacial engineering using self-assembling monolayer, J. Am. Chem. Soc. 137 (2015) 2674−2679.

[176] A. Yella, L.-P. Heiniger, P. Gao, M.K. Nazeeruddin, M. Grätzel, Nanocrystalline rutile electron extraction layer enables low-temperature solution

processed perovskite photovoltaics with 13.7% efficiency, Nano Lett. 14 (2014) 2591−2596.

[177] Z. Ren, A. Ng, Q. Shen, H.C. Gokkaya, J. Wang, L. Yang, W.-K. Yiu, G. Bai, A.B. Djurišić, W.W. Leung, Thermal assisted oxygen annealing for high efficiency planar $CH_3NH_3PbI_3$ perovskite solar cells, Sci. Rep. 4 (2014) 6752.

[178] P. Nagarjuna, P.N. Kumar, S.P. Singh, M. Deepa, M.A.G. Namboothiry, Efficient organic−inorganic hybrid perovskite solar cells processed in air, Phys. Chem. Chem. Phys. 16 (2014) 24691−24696.

[179] A. Huang, J. Zhu, J. Zheng, Y. Yu, Y. Liu, S. Yang, S. Bao, L. Lei, P. Jin, Room-temperature processible TiO_2 electron selective layers with controllable crystallinity for high efficiency perovskite photovoltaics, Sol. Energy Mater. Sol. Cell. 163 (2017) 15−22.

[180] Y. Wang, X. Zhan, Layer-by-Layer processed organic solar cells, Adv. Energy Mater. 6 (2016).

[181] A. Kogo, Y. Sanehira, Y. Numata, M. Ikegami, T. Miyasaka, Amorphous metal oxide blocking layers for highly efficient low temperature brookite TiO_2-based perovskite solar cells, ACS Appl. Mater. Interfaces (2018).

[182] T. Su, T. Hsieh, T. Wei, Electrodeposited TiO_2 film with mossy nanostructure for efficient compact layer in scaffold type perovskite solar cell, Sol. RRL (2018), 1700120 .

[183] M.-S. Wu, C.-H. Tsai, T.-C. Wei, Anodic deposition of ultrathin TiO_2 film with blocking layer and anchoring layer for dye-sensitized solar cells, J. Electrochem. Soc. 159 (2011) B80−B85.

[184] S. Rühle, D. Cahen, Electron tunneling at the TiO_2/substrate interface can determine dye-sensitized solar cell performance, J. Phys. Chem. B 108 (2004) 17946−17951.

[185] Y. Wang, J. Chang, L. Zhu, X. Li, C. Song, J. Fang, Electron-transport-layer-assisted crystallization of perovskite films for high-efficiency planar heterojunction solar cells, Adv. Funct. Mater. (2018).

[186] P. Liang, C. Liao, C. Chueh, F. Zuo, S.T. Williams, X. Xin, J. Lin, A.K. Jen, Additive enhanced crystallization of solution-processed perovskite for highly efficient planar-heterojunction solar cells, Adv. Mater. 26 (2014) 3748−3754.

[187] X. Deng, G.C. Wilkes, A.Z. Chen, N.S. Prasad, M.C. Gupta, J.J. Choi, Room-temperature processing of TiO_x electron transporting layer for perovskite solar cells, J. Phys. Chem. Lett. 8 (2017) 3206−3210.

[188] C. Sanchez, J. Livage, M. Henry, F. Babonneau, Chemical modification of alkoxide precursors, J. Non-Cryst. Solids 100 (1988) 65−76.

[189] J.I. Yajun, Growth mechanism and photocatalytic performance of double-walled and bamboo-type TiO_2 nanotube arrays, RSC Adv. 4 (2014) 40474−40481.

[190] H.-S. Kim, C.-R. Lee, J.-H. Im, K.-B. Lee, T. Moehl, A. Marchioro, S.-J. Moon, R. Humphry-Baker, J.-H. Yum, J.E. Moser, Lead iodide perovskite sensitized all-solid-state submicron thin film mesoscopic solar cell with efficiency exceeding 9%, Sci. Rep. 2 (2012) 591.

[191] J. Burschka, N. Pellet, S.-J. Moon, R. Humphry-Baker, P. Gao, M.K. Nazeeruddin, M. Grätzel, Sequential deposition as a route to high-performance perovskite-sensitized solar cells, Nature 499 (2013) 316.

[192] T.-S. Su, T.-Y. Hsieh, C.-Y. Hong, T.-C. Wei, Electrodeposited ultrathin TiO_2 blocking layers for efficient perovskite solar cells, Sci. Rep. 5 (2015) 16098.

[193] W. Ke, G. Fang, J. Wang, P. Qin, H. Tao, H. Lei, Q. Liu, X. Dai, X. Zhao, Perovskite solar cell with an efficient TiO_2 compact film, ACS Appl. Mater. Interfaces 6 (2014) 15959−15965.

[194] B. Xia, Z. Wu, H. Dong, J. Xi, W. Wu, T. Lei, K. Xi, F. Yuan, B. Jiao, L. Xiao, Formation of ultrasmooth perovskite films toward highly efficient inverted planar heterojunction solar cells by micro-flowing anti-solvent deposition in air, J. Mater. Chem. 4 (2016) 6295−6303.

[195] J. Xi, Z. Wu, K. Xi, H. Dong, B. Xia, T. Lei, F. Yuan, W. Wu, B. Jiao, X. Hou, Initiating crystal growth kinetics of α-HC $(NH_2)_2PbI_3$ for flexible solar cells with long-term stability, Nano Energy 26 (2016) 438−445.

[196] G.D. Rajmohan, F.Z. Huang, R. d'Agostino, J. du Plessis, X.J. Dai, Low temperature reactively sputtered crystalline TiO_2 thin film as effective blocking layer for perovskite solar cells, Thin Solid Films 636 (2017) 307−313.

[197] M. Kaltenbrunner, M.S. White, E.D. Głowacki, T. Sekitani, T. Someya, N.S. Sariciftci, S. Bauer, Ultrathin and lightweight organic solar cells with high flexibility, Nat. Commun. 3 (2012) 770.

[198] Y. Du, H. Cai, H. Wen, Y. Wu, L. Huang, J. Ni, J. Li, J. Zhang, Novel combination of efficient perovskite solar cells with low temperature processed compact TiO_2 layer via anodic oxidation, ACS Appl. Mater. Interfaces 8 (2016) 12836−12842.

[199] C. Ruan, M. Paulose, O.K. Varghese, G.K. Mor, C.A. Grimes, Fabrication of highly ordered TiO_2 nanotube arrays using an organic electrolyte, J. Phys. Chem. B 109 (2005) 15754−15759.

[200] P. Roy, S. Berger, P. Schmuki, TiO_2 nanotubes: synthesis and applications, Angew. Chem. Int. Ed. 50 (2011) 2904−2939.

[201] J. Wang, L. Liu, S. Liu, L. Yang, B. Zhang, S. Feng, J. Yang, X. Meng, W. Fu, H. Yang, Influence of a compact CdS layer on the photovoltaic performance of perovskite-based solar cells, Sustain. Energy Fuels 1 (2017) 504−509.

[202] Q. Zhang, C.S. Dandeneau, X. Zhou, G. Cao, ZnO nanostructures for dye-sensitized solar cells, Adv. Mater. 21 (2009) 4087−4108.

[203] I. Gonzalez-Valls, M. Lira-Cantu, Vertically-aligned nanostructures of ZnO for excitonic solar cells: a review, Energy Environ. Sci. 2 (2009) 19−34.

[204] J.B. Baxter, E.S. Aydil, Nanowire-based dye-sensitized solar cells, Appl. Phys. Lett. 86 (2005) 53114.

[205] A.E. Shalan, S. Narra, T. Oshikiri, K. Ueno, X. Shi, H.-P. Wu, M.M. Elshanawany, E.W.-G. Diau, H. Misawa, Optimization of a compact layer of TiO_2 via atomic-layer deposition for high-performance perovskite solar cells, Sustain. Energy Fuels 1 (2017) 1533−1540.

[206] X. Shi, K. Ueno, T. Oshikiri, H. Misawa, Improvement of plasmon-enhanced photocurrent generation by interference of TiO_2 thin film, J. Phys. Chem. C 117 (2013) 24733−24739.

[207] K. Nakamura, T. Oshikiri, K. Ueno, Y. Wang, Y. Kamata, Y. Kotake, H. Misawa, Properties of plasmon-induced photoelectric conversion on a TiO_2/NiO p−n junction with Au nanoparticles, J. Phys. Chem. Lett. 7 (2016) 1004−1009.

[208] S.M. George, Atomic layer deposition: an overview, Chem. Rev. 110 (2009) 111−131.

[209] E.H. Anaraki, A. Kermanpur, L. Steier, K. Domanski, T. Matsui, W. Tress, M. Saliba, A. Abate, M. Grätzel, A. Hagfeldt, Highly efficient and stable planar perovskite solar cells by solution-processed tin oxide, Energy Environ. Sci. 9 (2016) 3128−3134.

[210] S. Hong, A. Han, E.C. Lee, K.-W. Ko, J.-H. Park, H.-J. Song, M.-H. Han, C.-H. Han, A facile and low-cost fabrication of TiO_2 compact layer for efficient perovskite solar cells, Curr. Appl. Phys. 15 (2015) 574−579.

[211] L. Huang, C. Li, X. Sun, R. Xu, Y. Du, J. Ni, H. Cai, J. Li, Z. Hu, J. Zhang, Efficient and hysteresis-less pseudo-planar heterojunction perovskite solar cells fabricated by a facile and solution-saving one-step dip-coating method, Org. Electron. 40 (2017) 13−23.

[212] P. Ledezma, J. Jermakka, J. Keller, S. Freguia, Impact of film thickness of ultra-thin dip-coated compact TiO2 layers on the performance of mesoscopic perovskite solar cells, Masood, Muhammad Talha; Weinberger, Christian; Sarfraz, Jawad; Rosqvist, Emil; Sandén, Simon; Sandberg, Oskar; Vivo, Paola; Hashmi, Ghufran; Lund, Peter D.; Österbacka, Ronald; Smått, Jan-Henrik. In: ACS Applied Materials and Interfaces, Vol. 9, No. 21, 31.05. 2017, p. 17906-17913. Research output: Scientific-peer-review⟩ Article, Front. Microbiol. 8 (2017) 750.

[213] P. Vivo, A. Ojanperä, J.-H. Smått, S. Sandén, S.G. Hashmi, K. Kaunisto, P. Ihalainen, M.T. Masood, R. Österbacka, P.D. Lund, Influence of TiO_2 compact layer precursor on the performance of perovskite solar cells, Org. Electron. 41 (2017) 287−293.

[214] M. Liu, M.B. Johnston, H.J. Snaith, Efficient planar heterojunction perovskite solar cells by vapour deposition, Nature 501 (2013) 395−398.

[215] D. Zhao, W. Ke, C.R. Grice, A.J. Cimaroli, X. Tan, M. Yang, R.W. Collins, H. Zhang, K. Zhu, Y. Yan, Annealing-free efficient vacuum-deposited planar perovskite solar cells with evaporated fullerenes as electron-selective layers, Nano Energy 19 (2016) 88−97.

[216] X. Zhang, T. Wu, X. Xu, L. Zhang, J. Tang, X. He, J. Wu, Z. Lan, Ligand-exchange TiO_2 nanocrystals induced formation of high-quality electron transporting layers at low temperature for efficient planar perovskite solar cells, Sol. Energy Mater. Sol. Cell. 178 (2018) 65−73.

[217] S. O'Brien, L. Brus, C.B. Murray, Synthesis of monodisperse nanoparticles of barium titanate: toward a generalized strategy of oxide nanoparticle synthesis, J. Am. Chem. Soc. 123 (2001) 12085−12086.

[218] I. Bilecka, I. Djerdj, M. Niederberger, One-minute synthesis of crystalline binary and ternary metal oxide nanoparticles, Chem. Commun. (2008) 886−888.

[219] M. Abulikemu, M. Neophytou, J.M. Barbé, M.L. Tietze, A. El Labban, D.H. Anjum, A. Amassian, I. McCulloch, S. Del Gobbo, Microwave-synthesized tin oxide nanocrystals for low-temperature solution-processed planar junction organo-halide perovskite solar cells, J. Mater. Chem. 5 (2017) 7759−7763.

[220] W.L. Leong, Z. Ooi, D. Sabba, C. Yi, S.M. Zakeeruddin, M. Graetzel, J.M. Gordon, E.A. Katz, N. Mathews, Identifying fundamental limitations in halide perovskite solar cells, Adv. Mater. 28 (2016) 2439−2445.

[221] J.H. Heo, S.H. Im, J.H. Noh, T.N. Mandal, C.-S. Lim, J.A. Chang, Y.H. Lee, H. Kim, A. Sarkar, M.K. Nazeeruddin, Efficient inorganic-organic hybrid heterojunction solar cells containing perovskite compound and polymeric hole conductors, Nat. Photon. 7 (2013) 486−491.

[222] L.C. De Jonghe, M.N. Rahaman, 4.1 sintering of ceramics, Handb. Adv. Ceram. Mater. Appl. Proc. Prop. 2 (2003) 187.

[223] S. Li, Y. Zhao, X. Gu, Y. Qiang, N. Tan, Improved performance of perovskite solar cells by optimizing deposition parameters of TiO_2 compact layers, J. Mater. Sci. Mater. Electron. 28 (2017) 13626−13632.

[224] Z. Starowicz, K. Gawlińska, J. Walter, R.P. Socha, G. Kulesza-Matlak, M. Lipiński, Extended investigation of sol aging effect on TiO_2 electron transporting layer and performances of perovskite solar cells, Mater. Res. Bull. 99 (2018) 136−143.

[225] C. Zhang, Y. Luo, X. Chen, W. Ou-Yang, Y. Chen, Z. Sun, S. Huang, Influence of different TiO_2 blocking films on the photovoltaic performance of perovskite solar cells, Appl. Surf. Sci. 388 (2016) 82−88.